cmgh
CELLULAR AND MOLECULAR GASTROENTEROLOGY AND HEPATOLOGY

ORIGINAL RESEARCH

Paraspeckle Promotes Hepatocellular Carcinoma Immune Escape by Sequestering IFNGR1 mRNA

Jie Zan,[1,a] Xuya Zhao,[3,a] Xiya Deng,[2] Hongda Ding,[6] Bi Wang,[5] Minyi Lu,[1] Zijing Wei,[4] Zhi Huang,[4,5] and Shuai Wang[2]

[1]School of Biomedical and Pharmaceutical Sciences, Guangdong University of Technology, Guangzhou; [2]School of Life Sciences, Westlake University, Hangzhou; [3]Department of Interventional Radiology, Affiliated Cancer Hospital of Guizhou Medical University, Guiyang; [4]Department of interventional radiology, the Affiliated Hosptial of Guizhou Medical University, Guiyang, China; [5]School of Basic Medical Science, Guizhou Medical University, Guiyang, China; and [6]Department of General Surgery, Shengjing Hospital of China Medical University, Shenyang, China

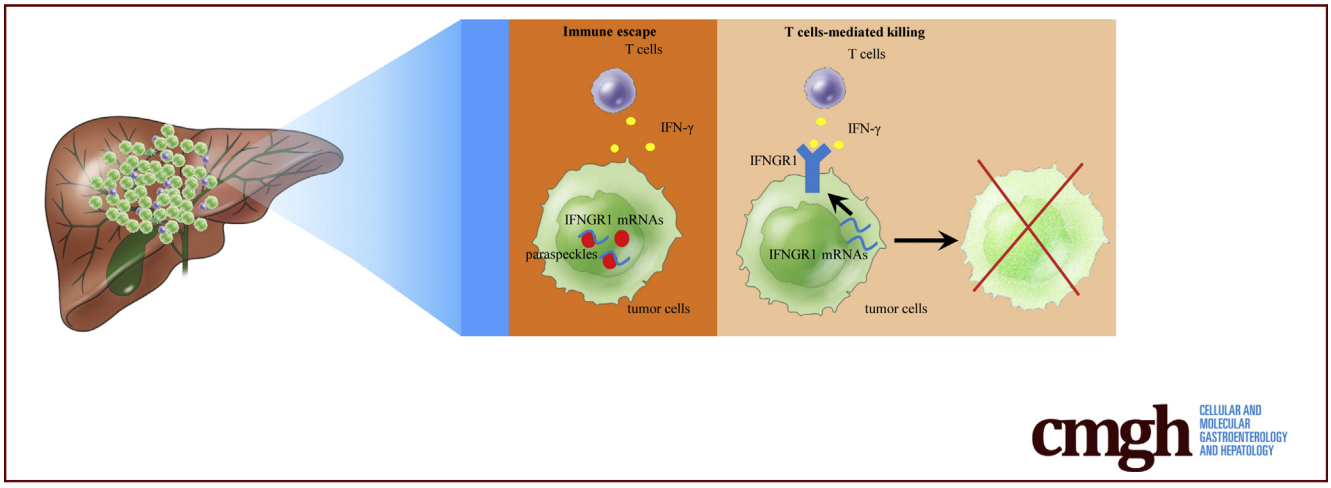

SUMMARY

Paraspeckle promotes hepatocellular carcinoma immune escape by sequestering IFNGR1 mRNA.

BACKGROUND & AIMS: Hepatocellular carcinoma (HCC) is the most common type of hepatic malignancies, with poor prognosis and low survival rate. Paraspeckles, which are unique subnuclear structures, are recently found to be involved in the development of various tumors, including HCC, and are related to induction in chemoresistance of HCC. This study aimed to investigate the possibility of paraspeckle in HCC cells participating in immune escape and its underlying mechanism in vitro and in vivo.

METHODS: Expression of NEAT1_2, the framework of paraspeckle, in HCC cells and tissues was detected by qRT-PCR and RNA-FISH. mRNAs interacted with NEAT1_2 were pull-downed and sequenced in C-terminal S1-aptamer-tagged NEAT1_2 endogenously expressed HCC cells constructed using CRISPR-CAS9 knock-in technology. The effects of paraspeckle on HCC sensitivity to T-cell-mediated cytolysis were detected by T-cell mediated tumor cell killing assay. The roles of NEAT1_2 or NONO on IFNGR1 expression and IFN-γ signaling by applying gene function loss analysis in HCC cells were detected by qRT-PCR, RNA immunoprecipitation, Western blotting, and ELISA. The role of paraspeckle during adoptive T-cell transfer therapy for HCC in vivo was performed with a subcutaneous xenograft mouse.

RESULTS: Paraspeckle in HCC cells is negatively related to T-cell-mediated cytolysis. Destruction of paraspeckle in HCC cells by knockdown of NEAT1_2 or NONO significantly improved the sensibility of resistant HCC cells to T-cell killing effects. Furthermore, IFNGR1 mRNA, which is sequestered by NEAT1_2 and NONO, is abundant in paraspeckle of T-cell killing-resistant HCC cells. Incapable IFN-γ-IFNGR1 signaling accounts for paraspeckle mediated-adoptive T-cell therapy resistance. Moreover, NEAT1_2 expression negatively correlates with IFNGR1 expression in clinical HCC tissues.

CONCLUSIONS: Paraspeckle in HCC cells helps tumor cells escape from immunosurveillance through sequestering IFNGR1 mRNA to inhibiting IFN-γ-IFNGR1 signaling, thereby avoiding T-cell killing effects. Collectively, our results hint that NEAT1_2 highly expressed HCC patient is more resistant to T-cell therapy in clinic, and NEAT1_2 may be potential target for HCC immunotherapy. *(Cell Mol Gastroenterol Hepatol 2021;12:465–487; https://doi.org/10.1016/j.jcmgh.2021.02.010)*

Keywords: Hepatocellular Carcinoma; Immunotherapy; Paraspeckle; Long Non-coding RNA Nuclear Enriched Abundant Transcript 1; Non-POU Domain-Containing Octamer-Binding Protein; Interferon Gamma Receptor 1.

Hepatocellular carcinoma (HCC) is the fourth most common cancer in terms of cancer-related mortality, causing more than 850,000 deaths globally each year.[1,2] Although great developments have occurred in the treatment strategies of HCC, including surgical resection, radiation therapy, transarterial chemoembolization, liver transplantation, and systemic therapy, the therapeutic effects are still not satisfactory, and HCC patients still have low 5-year survival and high recurrence rate.[3–5] Thus, developing more effective therapeutic approaches for HCC is urgently needed.

Tumor immunotherapies using immune checkpoint blockades or chimeric antigen receptor-engineered T cells have become a research hotspot in the field of cancer therapy and have achieved great clinical benefits.[6,7] Several monoclonal antibodies (mAbs) targeting immune checkpoint inhibitors, such as cytotoxic T-lymphocyte–associated antigen 4, programmed death 1 (PD1), or programmed cell death-ligand 1 (PD-L1), have now been approved by the U.S. Food and Drug Administration to treat some cancers through rescuing the cytotoxic function of $CD8^+$ T cells.[8–10] Activated T cells provide anti-tumor effects by production of effector cytokines and cytotoxic molecules, including tumor necrosis factor α, interferon-γ (IFNγ), perforin, granzymes, and granulysin.[6,11,12] However, statistical analysis of recent clinical trials of patients with advanced HCC showed that anti-PD1 therapy only achieves a 16%–20% objective response rate.[13,14] Thus, it is necessary to explore the underlying mechanism in low $CD8^+$ T-cell responses in HCC with immunotherapy.

Paraspeckle is a unique subnuclear structure composed of RNA elements, primarily the long non-coding RNA (lncRNA) nuclear enriched abundant transcript 1 (NEAT1), associated with RNA binding proteins (RBPs), and is involved in various aspects of gene regulation.[15] LncRNA NEAT1 is composed of 2 isoforms NEAT1_1 and NEAT1_2, of which the latter is essential for the assembly of nuclear paraspeckle.[16] Among the RBPs associated with LncRNA NEAT1, non-POU domain-containing octamer-binding protein (NONO), splicing factor proline and glutamine-rich protein (SFPQ), and paraspeckle component 1 protein (PSPC1) are required for the production or stabilization of NEAT1_2 and essential for structural maintenance of nuclear paraspeckle.[17] Recently, lncRNA NEAT1_2 has been reported to be involved in the development of several cancers, including gallbladder cancer, breast cancer, colorectal cancer, and HCC.[18–21] In addition, nuclear paraspeckle is found to be close to induction in chemoresistance and prediction for poor survival of HCC,[22] and lncRNA NEAT1 is found to regulate malignant phenotype of cancer cell and cytotoxic T-cell infiltration in lung cancer.[23] However, whether paraspeckle is involved in immunotherapy for HCC is completely unknown.

In the present study, we investigated the possibility of paraspeckle participating in the response of HCC cells to T-cell–mediated cytolysis and its underlying mechanism in vitro and in vivo. We found that paraspeckle in HCC cells is negatively related to T-cell–mediated HCC cell killing. Destruction of paraspeckle in HCC cells by knockdown of NEAT1_2 or NONO significantly improved the sensibility of resistant HCC cells to T-cell killing effects. Furthermore, through RNA immunoprecipitation and sequencing, we found that interferon gamma receptor 1 (IFNGR1) mRNA, which is sequestered by NEAT1_2 and NONO, is abundant in paraspeckles of T-cell killing resistant HCC cells. Incapable IFN-γ-IFNGR1 signaling accounts for paraspeckle mediated-adoptive T-cell therapy resistance. Moreover, NEAT1_2 expression negatively correlates with IFNGR1 expression in clinical HCC tissues. Overall, our results suggest that HCC patients with NEAT1_2 high expression may be more resistant to immunotherapies and indicate paraspeckle is a potential therapeutic target for improving immunotherapy efficacy of HCC.

Results

Paraspeckle in HCC Cells Is Negatively Related to T-Cell–Mediated HCC Cell Killing Effects

To explore the possibility of paraspeckle participating in the response of HCC cells to T-cell–mediated cytolysis, we first examined the expression levels of lncRNA NEAT1_2, the framework of paraspeckle, in 13 HCC cell lines and normal liver cell line HL7702. The results showed that SKhep1, HCCLM3, PLCPRF5, and BEL7402 cells have higher NEAT1_2 expression than other HCC cell lines and normal liver cell line HL7702 (Figure 1*A*). Furthermore, T-cell–mediated tumor cell killing assay showed that SKhep1 and HCCLM3 cells were more resistant to human T-cell–mediated cytolysis than other HCC cell lines and normal liver cell line (Figure 1*B*). Then we analyzed the correlation of NEAT1_2 expression level and crystal violet staining intensity of leftover HCC cells after co-culture with activated T cells and found that NEAT1_2 expression was positively correlated with violet staining intensity of HCC cells ($R^2 = 0.5981$, $P < .01$) (Figure 1*C*). From these results, we speculated that the content of paraspeckle may be correlated

[a]Authors share co-first authorship.

Abbreviations used in this paper: **AAV, adeno-associated virus; CXLR4, C-X-C motif chemokine receptor 4; FISH, fluorescence in situ hybridization; HCC, hepatocellular carcinoma; IFN-γ, interferon γ; IFNGR1, interferon gamma receptor 1; IP, intraperitoneal; IRF9, interferon regulatory factor 9; ISG, IFN-stimulated gene; JAK-STAT, Janus kinase-signal transducer and activator of transcription; KO, knockout; lncRNA-NEAT1, long non-coding RNA nuclear enriched abundant transcript 1; mAb, monoclonal antibody; NEDD4-1, neuronally expressed developmentally down-regulated 4; NONO, non-POU domain-containing octamer-binding protein; PBS, phosphate-buffered saline; PD1, programmed death 1; PD-L1, programmed cell death-ligand 1; PSPC1, paraspeckle component 1 protein; qRT-PCR, quantitative real-time polymerase chain reaction; RBP, RNA binding protein; RIP, RNA immunoprecipitation; RRM, RNA recognition motif; SD, standard deviation; Ser, serine; SFPQ, splicing factor proline- and glutamine-rich protein; si, short interfering; SOCS1, suppressor of cytokine signaling 1; Thr, threonine; Tyr, tyrosine; WT, wild-type.**

Most current article

2352-345X
https://doi.org/10.1016/j.jcmgh.2021.02.010

with the killing effects of T cells on HCC cells. Subsequently, to visualize the discrepancy of paraspeckle content in T-cell killing sensitive or resistant HCC cells, cellular distributions of NEAT1_2 and NONO, which binds NEAT1_2 to promote paraspeckle particle initial formation,[17] were detected by immunofluorescent staining, and the results showed that T-cell killing resistant HCC cells such as HCCLM3, SKhep1, and BEL7402 had more paraspeckles than T-cell killing sensitive HCC cells including HB611, Hep3b, and HepG2 (Figure 1*D*). Moreover, we explored whether destruction of paraspeckle formation by knockdown of NEAT1_2 or NONO with specific small interfering (si) RNAs (Figure 1*E*–*G*) could rescue the sensibility of resistant HCC cells to T-cell killing effects. As shown in Figure 1*H*, destruction of paraspeckle significantly improved the sensibility of resistant HCC cells, such as HCCLM3 and SKhep1 cells, to T-cell killing effects. Overall, these results indicate that paraspeckle in HCC cells is negatively related to T-cell–mediated HCC cell killing effects.

IFNGR1 mRNA Is Abundant in Paraspeckle of T-Cell Killing Resistant HCC Cells

Next, to clarify how paraspeckle reverses the response of HCC cells to T-cell killing effects, C-terminal S1-aptamer-tagged NEAT1_2 endogenously expressed HCCLM3 and SKhep1 cell lines were constructed using CRISPR-CAS9 knock-in technology (Figure 2*A*). We first verified that S1-tag knock-in did not affect NEAT1_2 expression, proliferation, or apoptosis of HCCLM3 and SKhep1 cells (Figure 2*B*–*D*), and S1-tagged-NEAT1_2 could be purified by streptavidin magnetic beads specifically (Figure 2*B*). To further ensure that S1-tagged NEAT1_2 participates in paraspeckle formation, we performed RNA immunoprecipitation (RIP) assays by using anti-NONO antibody and found that NONO could interact with S1-tagged NEAT1_2 (Figure 3*A*). Through sequencing mRNAs potentially interacted with NEAT1_2 by S1-tag mediated purification, we found 339 overlapping mRNAs in SKhep1 and HCCLM3 (Figure 3*B*–*D*). Furthermore, Kyoto Encyclopedia of Genes and Genomes analysis showed that the 339 overlapping genes were most enriched in cancer-related pathways, immune-regulatory signaling, and cytokine signaling (Figure 3*E*). Interestingly, IFNGR1, which is essential for anti-tumor responses and required for immune therapies,[24,25] is among the top 10 enriched genes and specifically detected in S1-tagged-NEAT1_2 of HCCLM3 or SKhep1 cells (Figure 3*F* and *G*). Moreover, IFNGR1 mRNA was demonstrated to be preserved in paraspeckle particles by performing RIP using S1-tag mediated pull-down (Figure 3*H*) or using NONO antibody-mediated purification (Figure 3*I*) in HCCLM3 and SKhep1 cells, respectively. Overall, these results indicate that IFNGR1 mRNA is abundant in paraspeckle of T-cell killing resistant HCC cells.

Paraspeckle-Mediated Inhibiting IFNGR1 Expression Contributes to T-Cell Killing Resistance of HCC Cells

Because IFNGR1 mRNA is preserved in paraspeckle of HCC cells, we suspected that paraspeckle could regulate IFNGR1 expression by entrapping IFNGR1 mRNA. Knockdown of NEAT1_2 using 2 different siRNAs to destroy paraspeckle up-regulated IFNGR1 protein expression in HCCLM3 and SKhep1 cells (Figure 4*A*), which was also confirmed by flow cytometry analysis (Figure 4*B*). Furthermore, we explored whether paraspeckle could regulate IFNGR1 mRNA expression. Through examining the IFNGR1 mRNA levels from total cell lysate or cytoplasmic/nuclear lysate, respectively, we found destruction of paraspeckle formation did not affect total IFNGR1 mRNA expression level in HCCLM3 and SKhep1 cells (Figure 4*C*) but led to more IFNGR1 mRNA distribution in cytoplasm (Figure 4*D*).

Subsequently, we further examined whether IFNGR1 is involved in T-cell–mediated killing HCC responses. By using CRISPR/CAS9 method, we generated IFNGR1-knockout (KO) HCCLM3 and SKhep1 cell lines, which were confirmed by Western blotting and flow cytometry analysis (Figure 5*A* and *B*). As expected, IFNGR1-KO HCC cells were more resistant to T-cell killing effects but did not affect proliferation or apoptosis of HCC cells (Figure 5*C*–*E*), and NEAT1_2 knockdown did not further promote T-cell killing resistance of IFNGR1-KO HCC cells (Figure 5*F*), suggesting that paraspeckle-mediated T-cell killing resistance of HCC cells depends on IFNGR1 expression. Next, we further investigated the role of IFNGR1 in adoptive anti-tumor immunity in immunodeficient $RAG^{-/-}$ mouse with tumor xenograft model. Equal numbers of IFNGR1-wild type (WT) or IFNGR1-KO HCC cells were subcutaneously transplanted in $RAG^{-/-}$ mouse, and 12 days later activated T cells were intravenously injected. The results showed that mice transplanted with IFNGR1-KO HCC cells had larger tumor size than WT group, and adoptive T-cell transfer significantly decreased the tumor size of WT group but not IFNGR1-KO group (Figure 6*A* and *B*). Moreover, to ensure the role of paraspeckle during adoptive T-cell transfer therapy, $RAG^{-/-}$ mice were injected with adeno-associated virus (AAV)-shR-NEAT1_2 by tail vein injection every 4 days after 6 days of transplantation of IFNGR1-WT or IFNGR1-KO HCC cells. All mice were intravenously injected with activated T cells at 12 days after transplantation. As shown in Figure 6*C*–*E*, destruction of paraspeckle formation by AAV-shR-NEAT1_2 significantly reduced the tumor size of WT group after adoptive T-cell transfer therapy but had no evident effect on IFNGR1-KO group after adoptive T-cell transfer therapy. Taken together, these results indicate that paraspeckle-mediated inhibiting IFNGR1 expression contributes to T-cell killing resistance of HCC cells.

Incapable IFN-γ-IFNGR1 Signaling Accounts for Paraspeckle Mediated-Adoptive T-Cell Therapy Resistance

It is known that IFN-γ is an essential cytokine for T-cell–mediated anti-tumor effects, and all effects of IFN-γ are mediated by IFN-stimulated genes (ISGs) such as C-X-C motif chemokine receptor 4 (CXCR4), interferon regulatory factor 9 (IRF9), and suppressor of cytokine signaling 1 (SOCS1), which are induced through IFNGR1 followed by activation of the Janus kinase (JAK)-signal transducer and

activator of transcription (STAT) signaling.[26] Because paraspeckle inhibits IFNGR1 protein expression via sequestering IFNGR1 mRNA (Figure 3), we suspected that destruction of paraspeckle formation promotes activation of IFN-γ signaling. As shown in Figure 7*A* and *B*, NEAT1_2 knockdown significantly promoted STAT1 701tyr phosphorylation, an activation marker of IFN-γ signaling (Figure 7*A*), and increased CXCR4, IRF9, and SOCS1

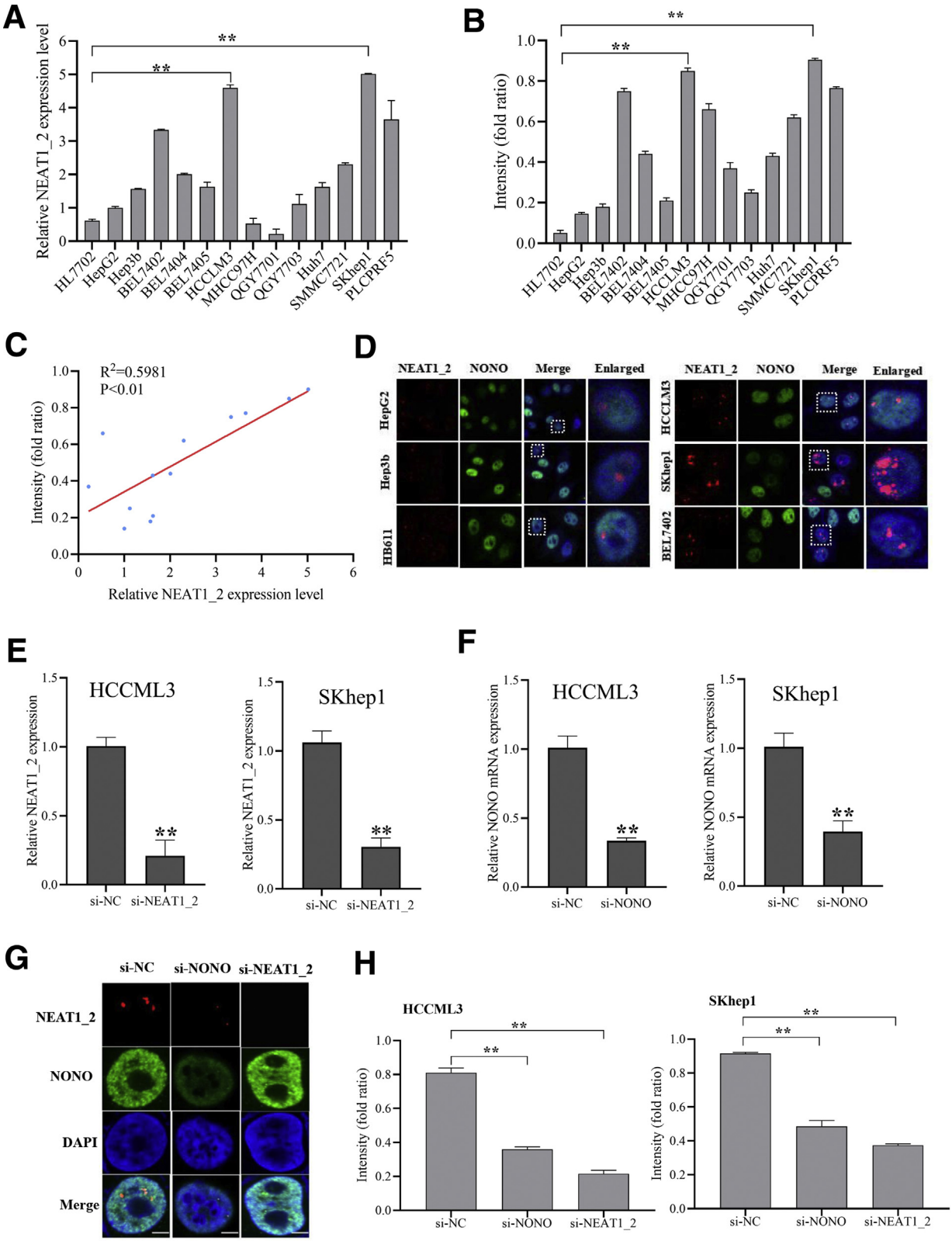

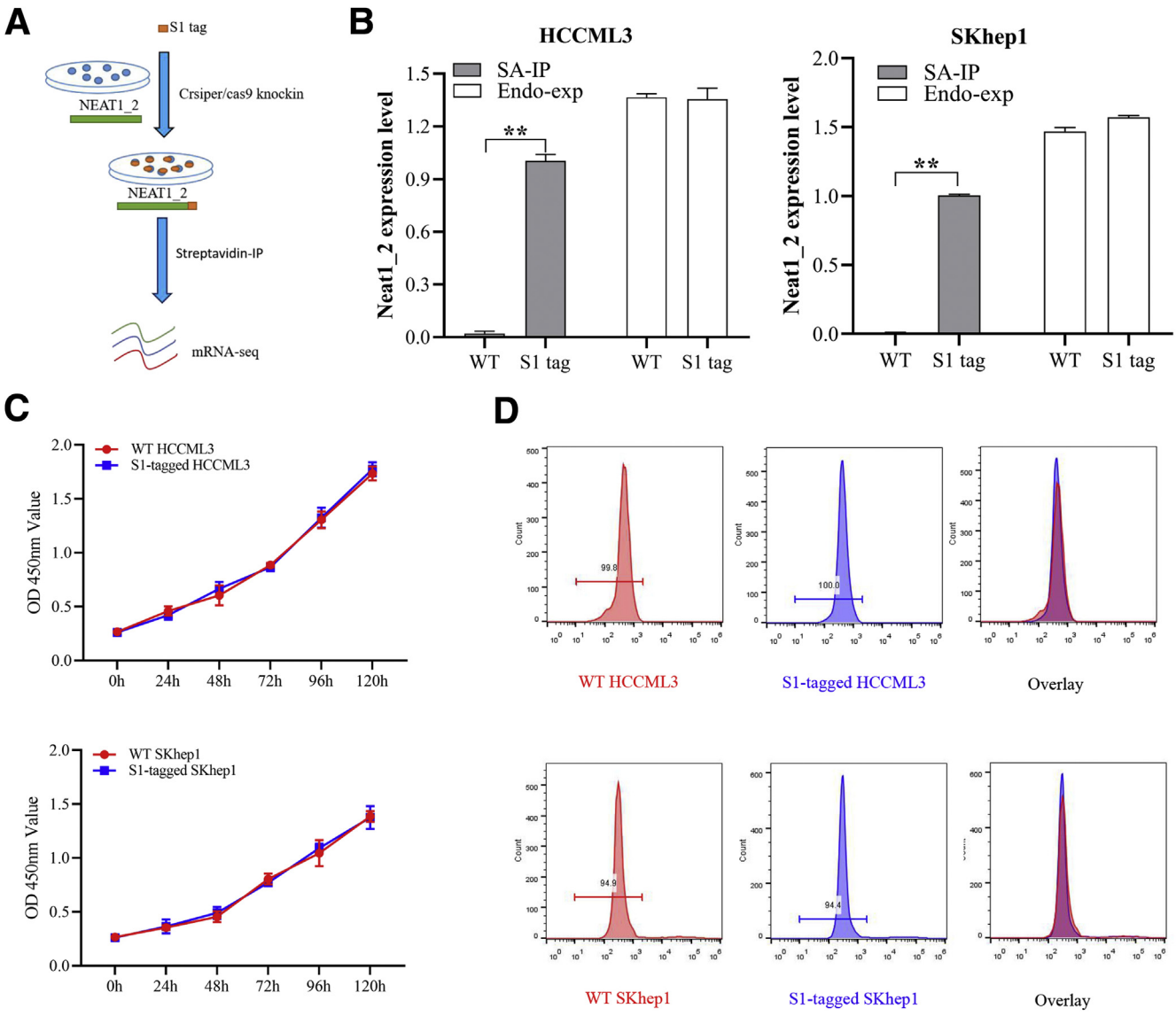

Figure 2. S1-tag knock-in did not affect NEAT1_2 expression, proliferation, or apoptosis of HCC cells. (*A*) Diagram of RIP-seq. (*B*) RIP analysis of NEAT1_2 relative expression in S1-tagged HCCML3 or SKhep1 cells with streptavidin (SA). Endogenous expression (Endo-exp) of NEAT1_2 was detected by qRT-PCR. (*C*) Proliferation of WT or S1-tagged HCCLM3 or SKhep1 cells was detected by MTT assay. (*D*) Apoptosis of WT or S1-tagged HCCLM3 or SKhep1 cells was detected by flow cytometry. Data are represented as means ± SD (n = 3; **P* < .05, ***P* < .01). IP, intraperitoneal.

expressions (Figure 7*B*). We also detected the transcription and secretion of IFN-γ and found destruction of paraspeckle formation promoted IFN-γ expression (Figure 7*C* and *D*). Next, we performed in vivo tumor xenograft experiments to investigate the role of IFN-γ-IFNGR1 signaling in paraspeckle-mediated adoptive anti-tumor immunity

Figure 1. (***See previous page***). **Paraspeckle in HCC cells is negatively related to T-cell–mediated HCC cell killing effects.** (*A*) Relative expression of NEAT1_2 in the indicated HCC cell lines and human normal liver cell line HL7702 were detected by qRT-PCR. (*B*) Response of HCC cells and normal liver cells HL7702 to T-cell–mediated cytolysis was detected by T-cell–mediated tumor cell killing assay. (*C*) Correlation analysis of relative expression of NEAT1_2 in HCC cells and response of HCC cells to T-cell–mediated cytolysis. (*D*) Cellular distribution of NEAT1_2 and NONO in the indicated HCC cells was detected by FISH and immunofluorescence assay. *White scale bar* in all images denotes 5 μm. (*E*) qRT-PCR analysis of knockdown efficacy of NEAT1_2 in HCCLM3 or SKhep1 cells. (*F*) qRT-PCR analysis of knockdown efficacy of NONO in HCCLM3 or SKhep1 cells. (*G*) Cellular distribution of NEAT1_2 and NONO in HCCML3 cells transfected with si-NC, si-NEAT1_2, or si-NONO was detected. (*H*) Response of HCCML3 or SKhep1 cells transfected with si-NC, si-NEAT1_2, or si-NONO to T-cell–mediated cytolysis was detected. Data are represented as means ± standard deviation (SD) (n = 3; **P* < .05, ***P* < .01).

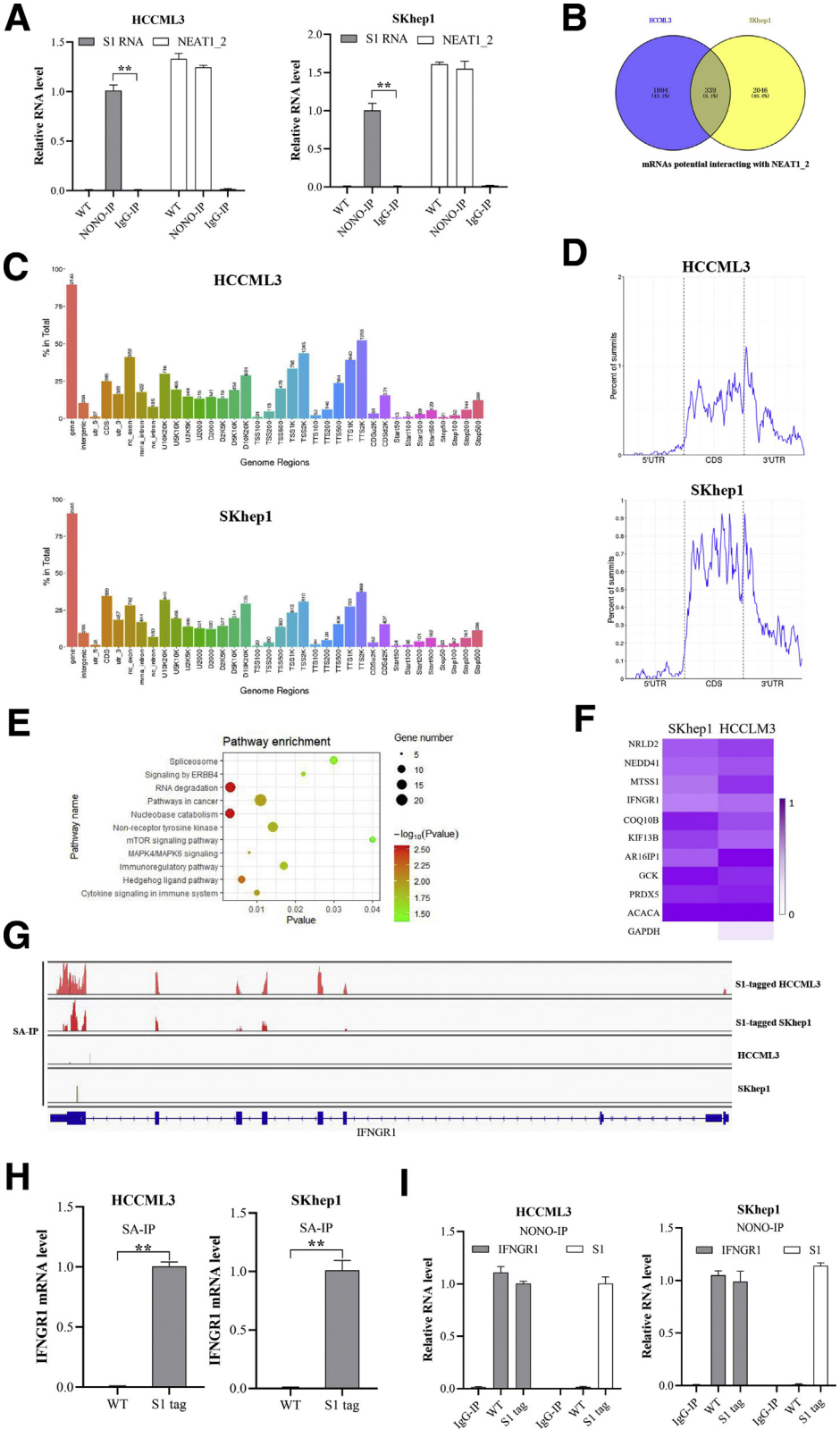

Figure 3. IFNGR1 mRNA is abundant in paraspeckle of T-cell killing resistant HCC cells. (*A*) RIP analysis of S1 or NEAT1_2 relative expression in S1-tagged HCCML3 or SKhep1 cells with anti-NONO antibody. (*B*) Venn diagram of mRNAs potentially interacted with NEAT1_2 in S1-tagged HCCML3 or SKhep1 cells, determined by RIP-seq by precipitation with streptavidin. (*C*) Genome regions of transcripts potentially interacted with NEAT1_2 in S1-tagged HCCML3 or SKhep1 cells. (*D*) Binding regions of transcripts potentially interacted with NEAT1_2 in S1-tagged HCCML3 or SKhep1 cells. (*E*) Kyoto Encyclopedia of Genes and Genomes analysis of the overlapped genes in Figure 2*B*. (*F*) Heatmap of the top 10 genes of the overlapped genes. (*G*) Assay for transposase accessible chromatin with RNA-seq at the IFNGR1 locus. (*H*) RIP analysis of S1-tagged NEAT1_2 interacted with IFNGR1 mRNA with streptavidin. (*I*) RIP analysis of NONO interacted with IFNGR1 mRNA or S1-tagged NEAT1_2 with anti-NONO antibody. Data are represented as means ± SD (n = 3; **P* < .05, ***P* < .01).

resistance in immunodeficient RAG$^{-/-}$ mouse model. The results showed that destruction of paraspeckle formation by AAV-shR-NEAT1_2 significantly reduced the tumor size under adoptive T-cell transfer therapy, compared with the control AAV-shR-NC group (Figure 8*A* and *B*), whereas blocking IFNGR1 with anti-IFNGR1 mAb evidently abolished the therapeutic effect of AAV-shR-NEAT1_2 injection (Figure 8*A* and *B*). In addition, to exclude the role of IFN-γ,

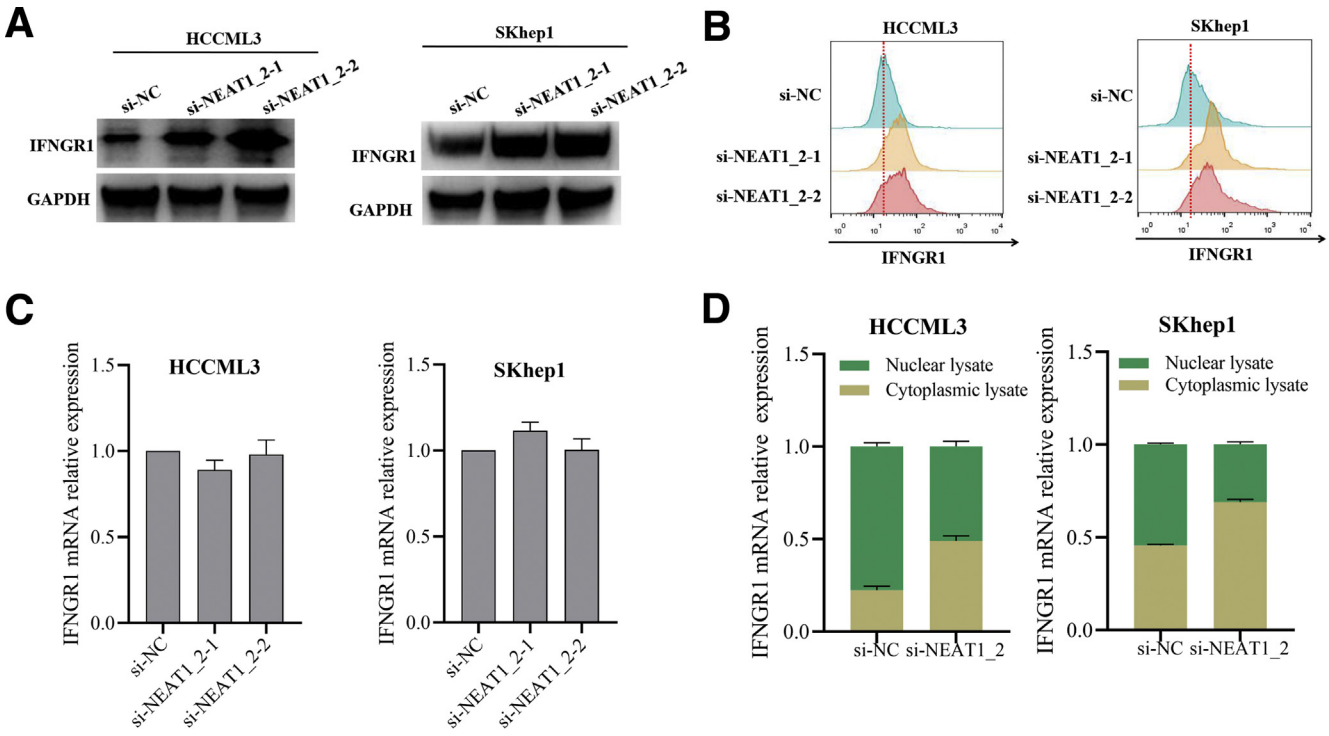

Figure 4. Destruction of paraspeckle promotes IFNGR1 expression in HCC cells. (*A* and *B*) IFNGR1 protein expressions in HCCML3 or SKhep1 cells transfected with si-NC or si-NEAT1_2 detected by Western blotting (*A*) and flow cytometry (*B*). (*C*) Relative expressions of IFNGR1 mRNA in HCCML3 or SKhep1 cells transfected with si-NC or si-NEAT1_2 detected by qRT-PCR. (*D*) Relative expressions of IFNGR1 mRNA in the cytoplasmic and nuclear fractions of HCCML3 or SKhep1 cells transfected with si-NC or si-NEAT1_2 detected by qRT-PCR. Data are represented as means ± SD (n = 3).

we used anti-IFN-γ mAb to neutralize IFN-γ by intraperitoneal injection. As shown in Figure 8*C* and *D*, IFN-γ neutralization also abolished the therapeutic effect of AAV-shR-NEAT1_2 injection. Taken together, these results indicate that incapable IFN-γ-IFNGR1 signaling accounts for paraspeckle mediated-adoptive T-cell therapy resistance.

NONO Mediates Retention of IFNGR1 mRNA in Paraspeckle in HCC Cells

Paraspeckle is composed of RNA elements, primarily lncRNA NEAT1_2 and several RBPs, among which NONO is highly abundant and essential for paraspeckle assembly.[15] Next, we explored whether NEAT1_2 binding to IFNGR1 mRNA depends on other RBPs. To confirm our speculation, we performed RIP with proteinase K treatment to eliminate the effects of proteins and found proteinase K treatment abolished the binding between NEAT1_2 and IFNGR1 mRNA (Figure 9*A*). NONO knockdown also significantly reduced the amounts of IFNGR1 mRNA binding to NEAT1_2 (Figure 9*B*), indicating that NONO partially mediates the binding between NEAT1_2 and IFNGR1 mRNA. Furthermore, we performed segmental RIP to detect the regions of NEAT1_2 associated with NONO and found that NONO mainly bound to the region 13-15 of NEAT1_2 (Figure 9*C*), which is consistent to previous structural data.[27] Subsequently, we generated NEAT1_2 region 13-15-KO WT or S1-tagged HCCLM3 and SKhep1 cell lines by CRISPR/CAS9 method (Figure 9*D*) and found that KO of region 13-15 of NEAT1_2 did not significantly affect the proliferation or apoptosis of HCC cells (Figure 9*E* and *F*) but evidently abolished the binding between NEAT1_2 and IFNGR1 mRNA (Figure 9*G*). Moreover, to identify the domain of NONO responsible for binding to IFNGR1 mRNA, we constructed a series of NONO truncated plasmids and found that RNA recognition motifs (RRMs) 1 and 2 of NONO are responsible for binding to IFNGR1 mRNA (Figure 9*H*). In addition, KO of NEAT1_2 region 13-15 also significantly inhibited NONO binding to IFNGR1 mRNA (Figure 9*I*), suggesting that NEAT1_2 interacting with NONO is essential for NONO associated with IFNGR1 mRNA.

Previous study reported that the RRMs of NONO include a threonine residue (Thr15) whose phosphorylation inhibits its RNA binding ability.[28] We further explored whether NEAT1_2 binding to NONO affects NONO chemical modification, which in tune regulates the RNA binding capacity of NONO. Because serine (Ser), Thr, and tyrosine (Tyr) phosphorylation are the most conventional chemical modification of amino acid, we detected phosphorylated Ser, Thr, and Tyr of NONO protein and found NEAT1_2 knockdown decreased phosphorylated Ser/Thr level but did not affect phosphorylated Tyr level (Figure 9*J*). Combined with the results of Figure 9*H* and previous study,[28] we speculated that ser147 in NONO RRM domain is the most possible modified amino acid. Then we mutated ser147 of NONO to alanine147 and found that mutation of ser147 blocked the

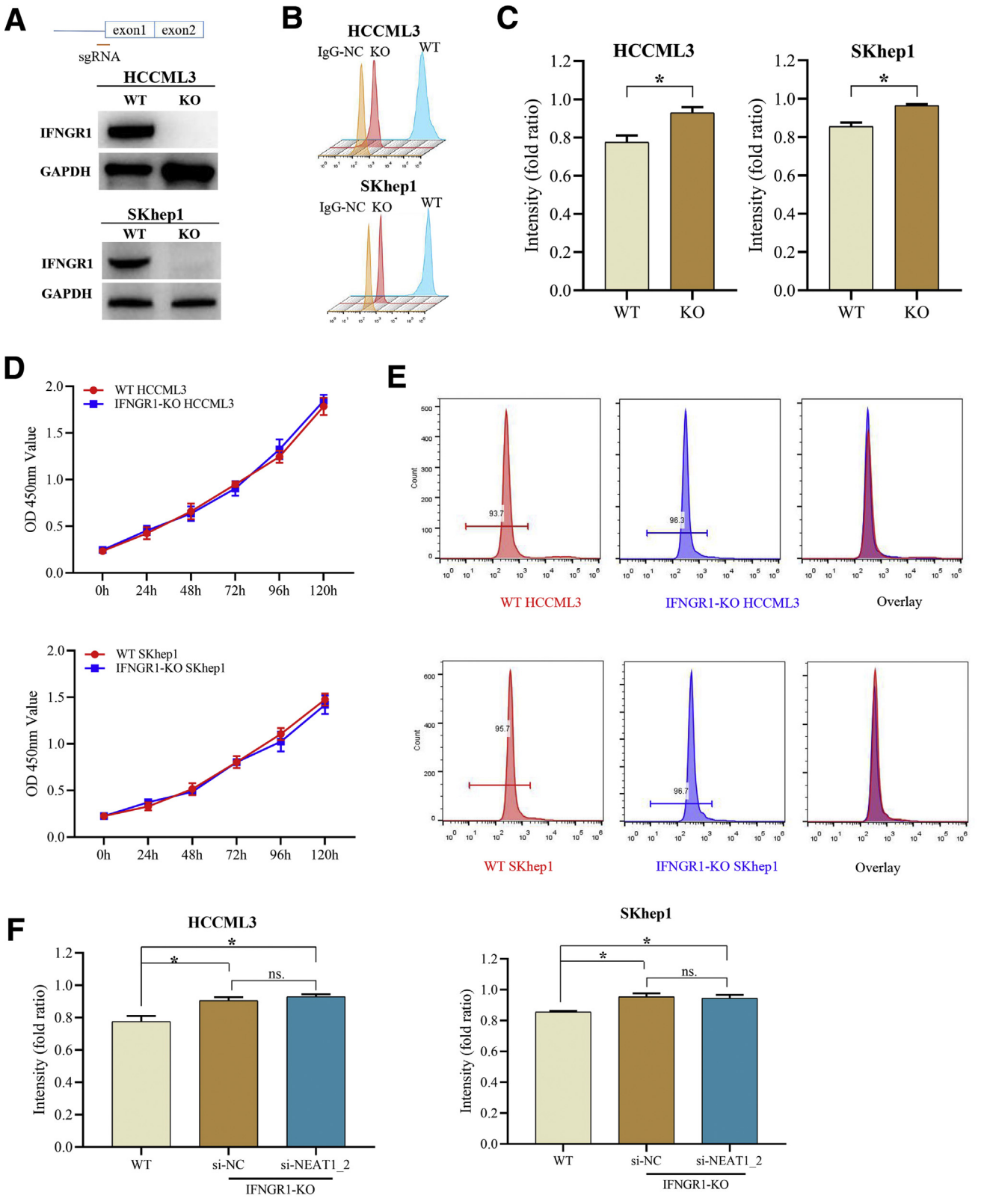

Figure 5. IFNGR1-KO HCC cells were more resistant to T-cell killing effects. (*A* and *B*) IFNGR1 protein expressions in IFNGR1-KO or WT HCCML3/SKhep1 cells detected by Western blotting (*A*) and flow cytometry (*B*). (*C*) Response of WT or IFNGR1-KO HCCML3/SKhep1 cells to T-cell–mediated cytolysis detected by T-cell–mediated tumor cell killing assay. (*D*) Proliferation of WT or IFNGR1-KO HCCLM3 or SKhep1 cells was detected by MTT assay. (*E*) Apoptosis of WT or IFNGR1-KO HCCLM3 or SKhep1 cells was detected by flow cytometry. (*F*) Response of IFNGR1-KO HCCML3 or SKhep1 cells transfected with si-NC or si-NEAT1_2 to T-cell–mediated cytolysis detected by T-cell–mediated tumor cell killing assay. Data are represented as means ± SD (n = 3; **P* < .05, ***P* < .01).

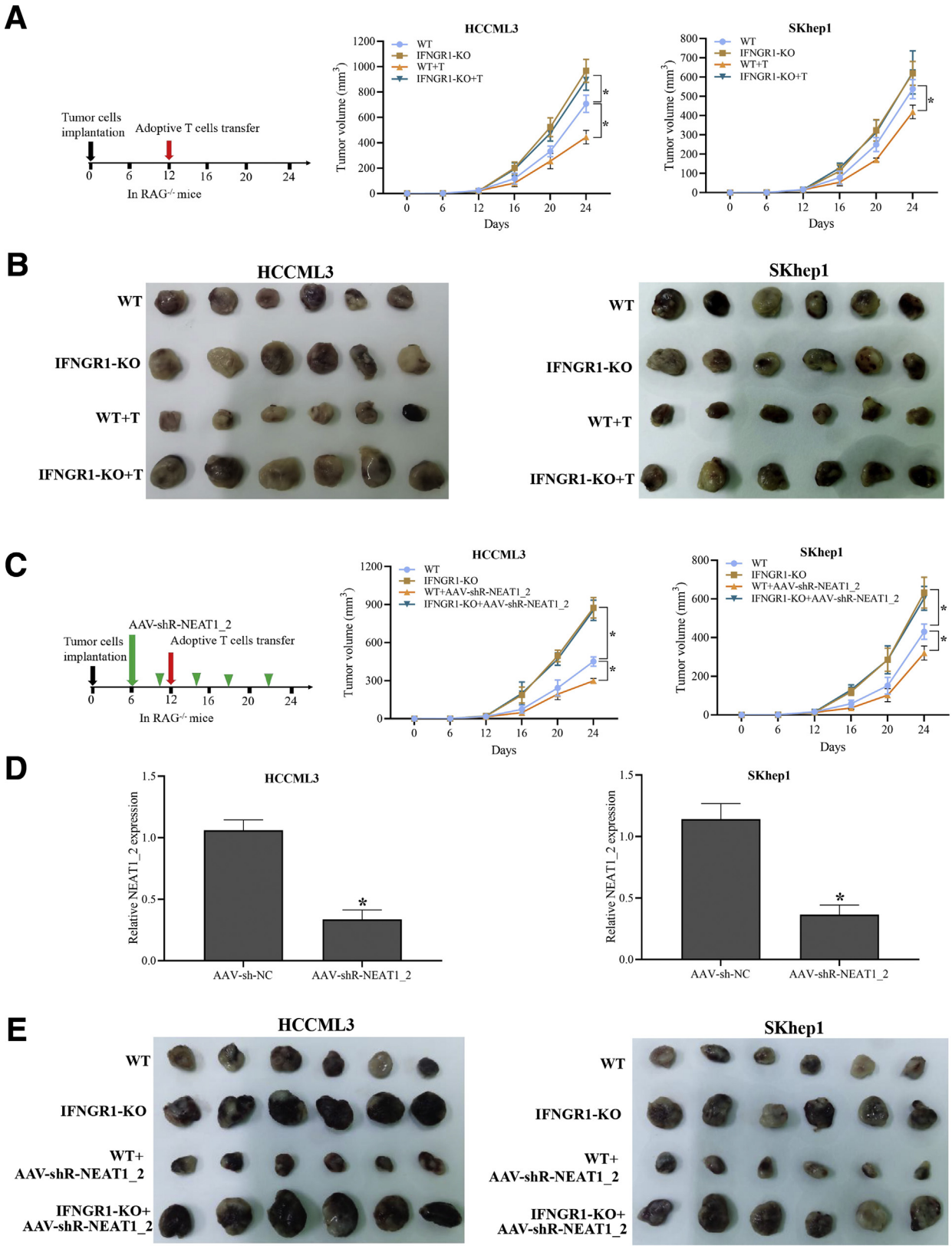

Figure 6. Paraspeckle-mediated inhibiting IFNGR1 expression contributes to T-cell killing resistance of HCC. (*A*) Schematic diagram of animal experimental protocols to assess effects of IFNGR1 KO on adoptive T-cell anti-tumor immunity in immunodeficient RAG$^{-/-}$ mouse (n = 6). Tumor growth curve of human HCC-bearing mice. (*B*) Image showing comparison of excised tumor size of HCCML3 xenografts in RAG1-/- mice. (*C*) Schematic diagram of animal experimental protocols to assess effects of NEAT1_2 knockdown on adoptive T-cell anti-tumor immunity in immunodeficient RAG$^{-/-}$ mouse (n = 6). Tumor growth curve of human HCC-bearing mice. (*D*) qRT-PCR analysis of knockdown efficacy of AAV-shNEAT1/2 in the tumor of HCC xenografts in RAG1-/- mice. (*E*) Image showing comparison of excised tumor size of SKhep1 xenografts in RAG1-/- mice. Data are represented as means ± SD (n = 6; **P* < .05, ***P* < .01).

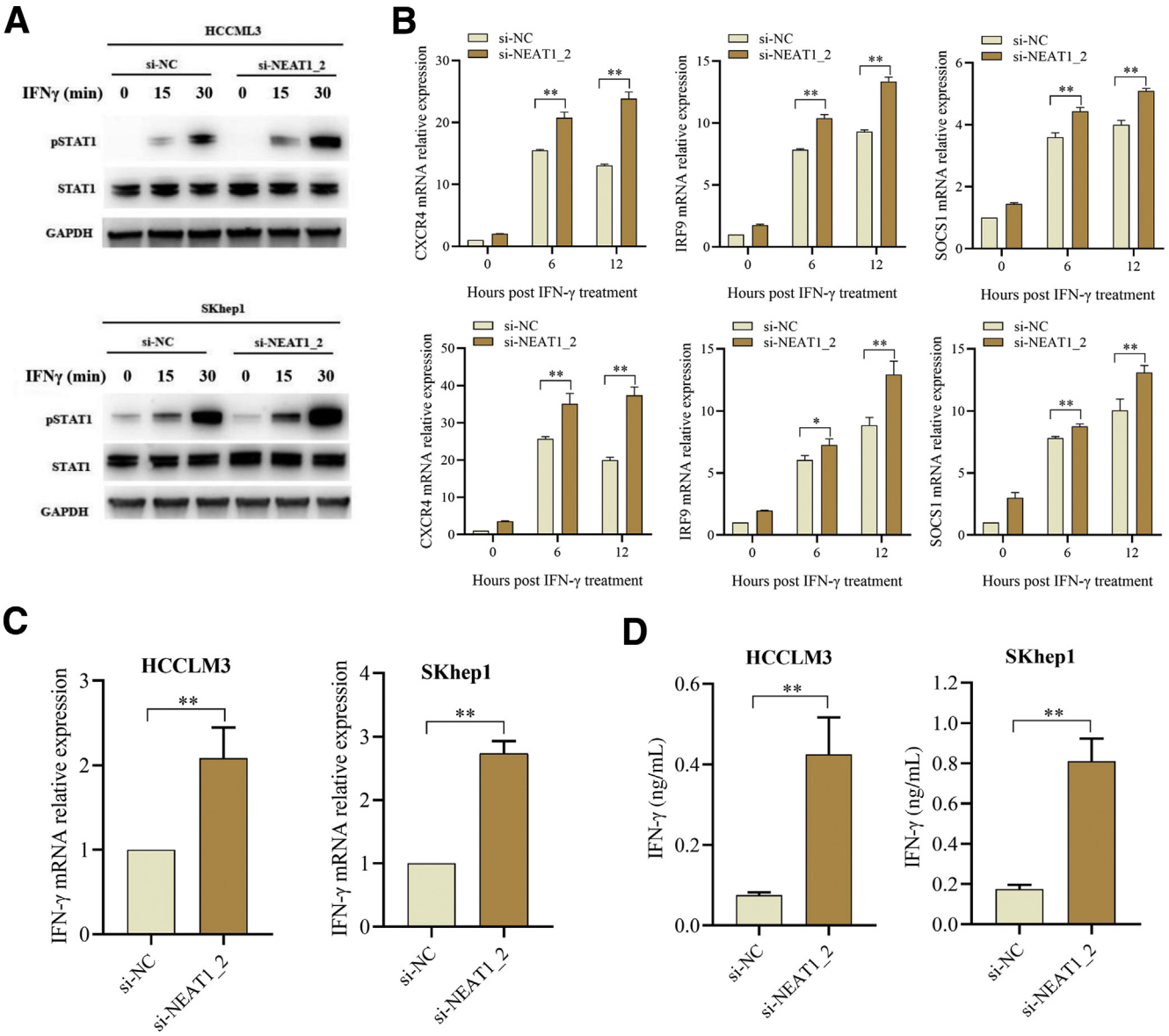

Figure 7. Destruction of paraspeckle promotes activation of IFN-γ signaling in HCC cells. (*A*) STAT3 and phosphorylated STAT3 (pSTAT3) protein expression levels in HCC cells transfected with si-NC or si-NEAT1_2 and treated with IFN-γ (100 ng/mL) were detected by Western blotting. (*B*) Relative mRNA expressions of CXCL4, IRF9, and SOCS1 in the indicated HCC cells were detected by qRT-PCR. (*C*) Relative mRNA expression of IFN-γ in indicated HCC cells was detected by qRT-PCR. (*D*) IFN-γ production in cultural supernatants of HCC cells was detected by enzyme-linked immunosorbent assay. Data are represented as means ± SD (n = 3; **P* < .05, ***P* < .01).

inhibitory effect of NEAT1_2 knockdown on Ser/Thr phosphorylation (Figure 9*K*). Moreover, mutation of ser147 also inhibited the binding between NONO and IFNGR1 mRNA (Figure 9*L*). Taken together, these results demonstrate that NEAT1_2 binding to NONO may promote NONO ser147 phosphorylation, which strengthens the interaction between NONO RRM domain and IFNGR1 mRNA.

NEAT1_2 Region 13-15 Is Essential for Paraspeckle-Mediated T-Cell Killing Tolerance

Next, we further explored whether the binding among NEAT1_2 region 13-15, NONO, and IFNGR1 mRNA affects IFNGR1 protein expression. As shown in Figure 10*A*, IFNGR1 protein expression levels were obviously upregulated in NEAT1_2 region 13-15 KO HCC cells, compared with those in WT HCC cells. In addition, NEAT1_2 region 13-15 KO did not significantly affect NONO protein expression in HCC cells (Figure 10*A*). Furthermore, NEAT1_2 region 13-15 KO also promoted IFN-γ secretion of HCC cells (Figure 10*B*) and evidently decreased the resistance of HCC cells to T-cell killing (Figure 10*C*). Then, we further investigated the role of NEAT1_2 region 13-15 KO in adoptive anti-tumor immunity in immunodeficient $RAG^{-/-}$ mouse with tumor xenograft model. As shown in Figure 10*D*, KO of NEAT1_2 region 13-15 significantly

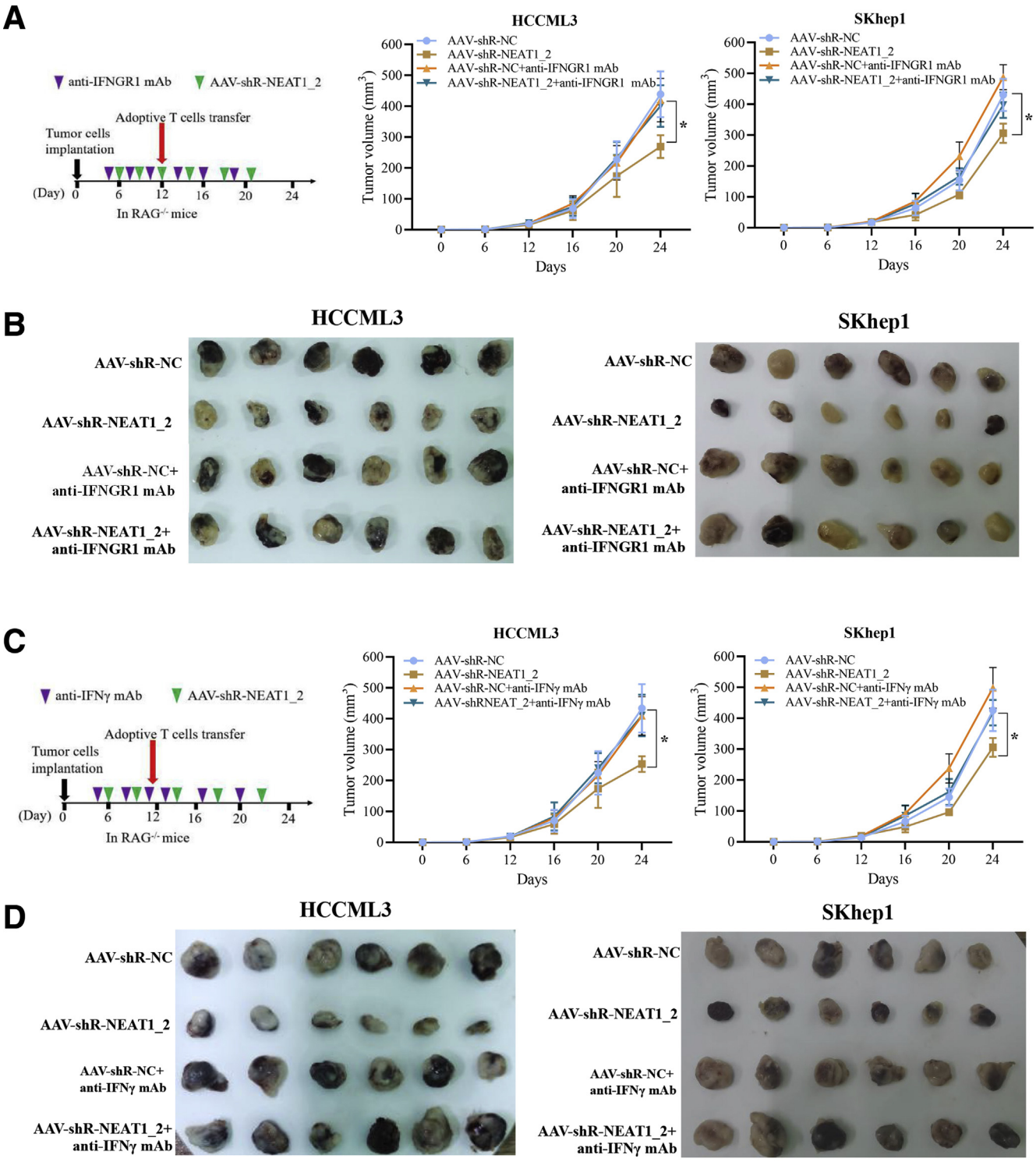

Figure 8. Incapable IFN-γ-IFNGR1 signaling accounts for paraspeckle mediated-adoptive T-cell therapy resistance. (*A*) Schematic diagram of animal experimental protocols to assess effects of blocking IFNGR1 with anti-IFNGR1 mAb on adoptive T-cell anti-tumor immunity in immunodeficient RAG-/- mouse (n = 6). Tumor growth curve of human HCC-bearing mice. (*B*) Image showing comparison of excised tumor size of HCC xenografts in RAG1-/- mice. (*C*) Schematic diagram of animal experimental protocols to assess effects of neutralizing IFN-γ with anti-IFN-γ mAb on adoptive T-cell anti-tumor immunity in immunodeficient RAG-/- mouse (n = 6). Tumor growth curve of human HCC-bearing mice. (*D*) Image showing comparison of excised tumor size of HCC xenografts in RAG1-/- mice. Data are represented as means ± SD (n = 6; $^{*}P < .05$, $^{**}P < .01$).

decreased the tumor size of HCC cells under adoptive T-cell transfer, whereas blocking IFNGR1 with anti-IFNGR1 mAb abolished the inhibitory effect of NEAT1_2 region-KO (Figure 10*E* and *F*). In addition, IFN-γ neutralization also abolished the therapeutic effect of NEAT1_2 region-KO (Figure 6*F*, Figure 10*G* and *H*). Taken together, these results indicate NEAT1_2 region 13-15 is essential for paraspeckle-mediated T-cell killing tolerance.

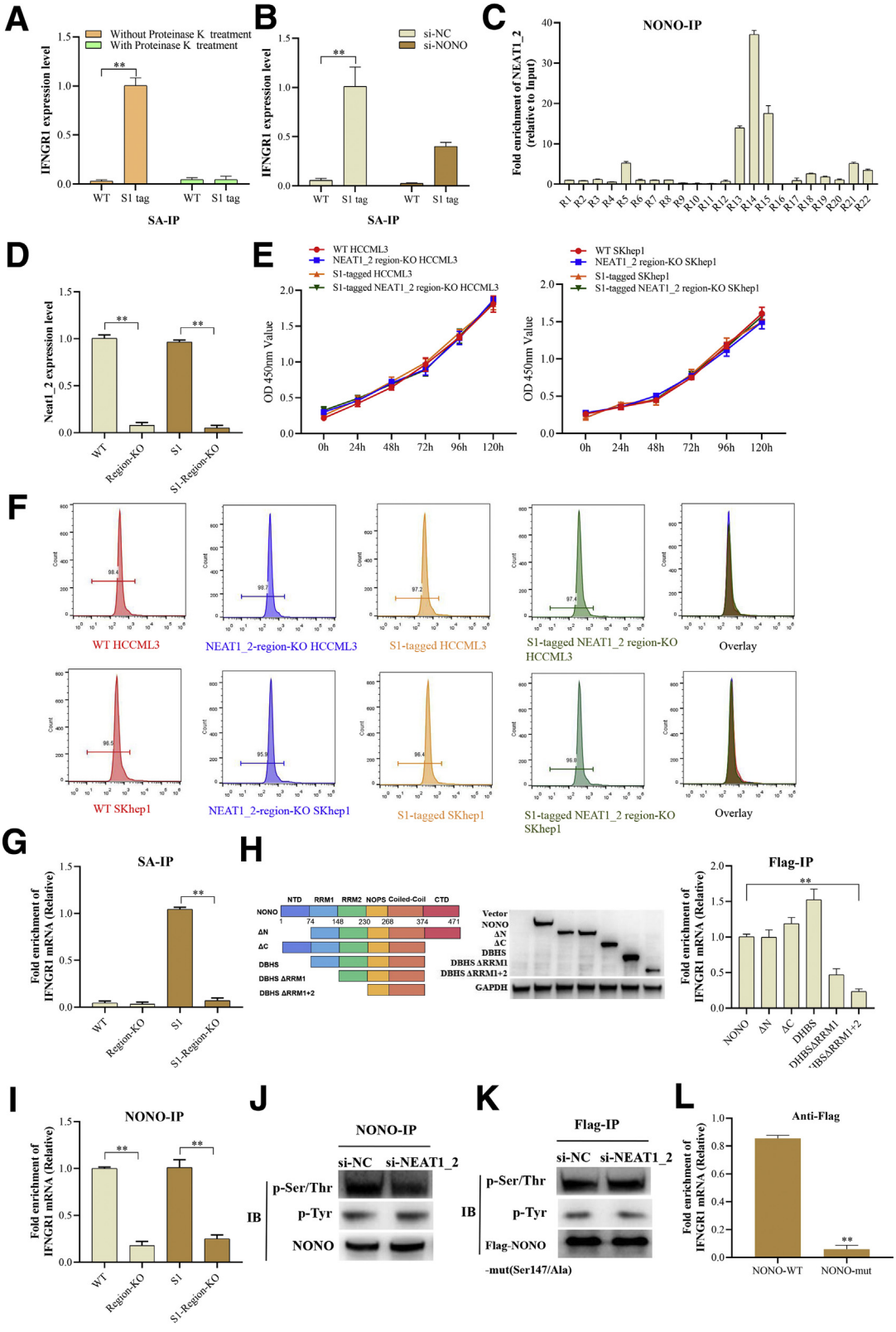

NEAT1_2 Expression Negatively Correlates With IFNGR1 Expression in Clinical Tumor Tissues

To expand our discovery, we first analyzed the co-relationship between NEAT1, NONO, and immune cell infiltration in HCC tissues using clinical database (TIMER). As shown in Figure 11*A* and *B*, the expression levels of NEAT1 and NONO had weak co-relationship with CD8+ T-cell infiltration, but NONO had common co-relationship with macrophage and dendritic cell infiltration. Then, through analyzing clinical HCC tissues (Table 2) using RNA fluorescence in situ hybridization (FISH), we classified HCC tissues as NEAT1_2 low expression group and NEAT1_2 high expression group (Figure 11*C*). T-cell infiltration was detected by using anti-CD3 and anti-CD8 antibodies through immunofluorescence, and we found there was no significant discrepancy of $CD3^+$ or $CD8^+$ T-cell infiltration between the 2 groups (Figure 11*D*), indicating that NEAT1_2 expression did not affect $CD8^+$ T-cell infiltration in HCC. However, through Pearson's correlation coefficient analysis, we found IFNGR1 protein levels were negatively correlated with NEAT1_2 RNA levels in HCC (Figure 11*E*, Figure 12). To further detect the activation status of IFN-γ-IFNGR1 signaling on HCC tissues, we also detected the downstream ISGs induced by IFN-γ and found that ISGs such as CXCR4, IRF9, and SOCS1 were higher expressed in NEAT1_2 low expression group, compared with those in NEAT1_2 high expression group (Figure 11*F*). Taken together, these results indicate the phenomenon of paraspeckle negatively related to IFNGR1 expression also exists in HCC tissues, which may hint NEAT1_2 highly expressed HCC patient is more resistant to T-cell therapy in clinic.

Discussion

HCC is the most common type of hepatic malignancies, with poor prognosis and low survival rate.[3] Recently, immunotherapies using immune checkpoint blockades or chimeric antigen receptor-modified T cells have achieved great clinical benefits for HCC patients.[7,29] However, during the process of immunosurveillance, HCC cells could escape immune attack through secreting immunosuppressive cytokines and manipulating immune checkpoint molecules.[30,31] Thus, clarifying the underlying mechanism in immune escape of HCC cells is essential for improving therapeutic effect of immunotherapies for HCC patients. In this study, we report that paraspeckle in HCC cells helps tumor cells escape from immunosurveillance through sequestering IFNGR1 mRNA to inhibiting IFN-γ-IFNGR1 signaling, thereby avoiding T-cell killing effects. In addition, we find that NEAT1_2, the framework of paraspeckle, negatively correlates with IFNGR1 expression in clinical HCC tissues, which may hint that HCC patients with NEAT1_2 high expression may be more resistant to immunotherapies.

Paraspeckle, which is a unique subnuclear structure, has been recently found to be involved in the development of various tumors.[32] For example, NEAT1_2 promotes gallbladder cancer, gastric cancer, breast cancer, and HCC progression through sponging miR-335, miR-497-5p, miR-107, or miR-296-5p, respectively.[18,33–35] In addition, paraspeckle has been shown to enhance chemoresistance in several cancer types including HCC.[22] In this study, we found paraspeckle of HCC cells is positively related to resistance to adoptive T-cell killing effects through retention of IFNGR1 mRNA, because destruction of paraspeckle by knockdown or KO of NEAT1_2 significantly promoted IFNGR1 protein expression, enhanced IFN-γ-IFNGR1 signaling, and activated downstream ISG transcription. Besides IFNGR1 mRNA, many other genes potentially interacted with NEAT1_2 were identified in HCC cells. For example, neuronally expressed developmentally down-regulated 4 (NEDD4, also known as NEDD4-1) E3 ligase plays a critical role in carcinogenesis via the ubiquitination-mediated degradation of multiple substrates.[36] Phosphorylated-AKT, as the substrate of NEDD4-1, has been reported to promote PD-L1 expression in cancers for immune suppression.[37,38] Whether NEDD4-1 or other genes are also involved in paraspeckle-mediated resistance to T-cell killing effects needs to be further explored in future studies.

NONO, which is required for stabilization of Neat1_2 and structural maintenance of nuclear paraspeckle, is involved in transcriptional control, transcription termination, and RNA processing and has been recently found to have participated in nuclear retention of hyperedited RNA.[39,40] We found that NONO specifically interacts with IFNGR1 mRNA via RRM domains, which is consistent with previous study that RRM domains are essential for NONO binding to RNAs.[28] The RRM domains preceded by an HQ-rich region

Figure 9. (***See previous page***). **NONO mediates retention of IFNGR1 mRNA in paraspeckle of HCC cells.** (*A*) RIP analysis of S1-tagged NEAT1_2 interacting with IFNGR1 mRNA in S1-tagged HCCML3 cells treated with proteinase K or not. (*B*) RIP analysis of S1-tagged NEAT1_2 interacting with IFNGR1 mRNA in S1-tagged HCCML3 cells transfected with si-NONO or si-NC. (*C*) RIP analysis of interacting regions of NEAT1_2 with NONO in HCCML3 cells. (*D*) qRT-PCR analysis of region 13-15 of NEAT1_2 expression in region 13-15 of NEAT1_2-KO HCCML3 cells. (*E*) Proliferation of WT or region 13-15 of NEAT1_2-KO HCCLM3 or SKhep1 cells was detected by MTT assay. (*F*) Apoptosis of WT or region 13-15 of NEAT1_2-KO HCCLM3 or SKhep1 cells was detected by flow cytometry. (*G*) RIP analysis of NEAT1_2 interacting with IFNGR1 mRNA in region 13-15 of NEAT1_2-KO HCCML3 cells using streptavidin. (*H*) Diagram of NONO domains (*left*). RIP analysis of interacting domains of NONO with IFNGR1 mRNA using anti-Flag antibody (*right*). (*I*) RIP analysis of NONO interacting with IFNGR1 mRNA in region 13-15 of NEAT1_2-KO HCCML3 cells using anti-NONO antibody. (*J*) Western blotting analysis of phosphorylated modifications of immunoprecipitated NONO using anti-NONO antibody in HCCML3 cells transfected with si-NONO or si-NC. (*K*) Western blotting analysis of phosphorylated modifications of immunoprecipitated Flag-NONO mutant using anti-Flag antibody in HCCML3 cells transfected with pcmv-Flag-NONO mutant vector and si-NONO or si-NC. (*L*) RIP analysis of NONO interacting with IFNGR1 mRNA in HCCML3 cells transfected with pcmv-Flag-NONO (WT) or NONO mutant using anti-Flag antibody. Data are represented as means ± SD (n = 3; $^*P < .05$, $^{**}P < .01$).

include a threonine residue (Thr15) whose phosphorylation inhibits NONO's RNA binding ability, except for G-rich RNAs such as NEAT1_2.[28] Here we found that knockdown of the region 13-15 of NEAT1_2 responsible for interacting with NONO significantly inhibited NONO binding to IFNGR1 mRNA, and knockdown of NEAT1_2 evidently decreased

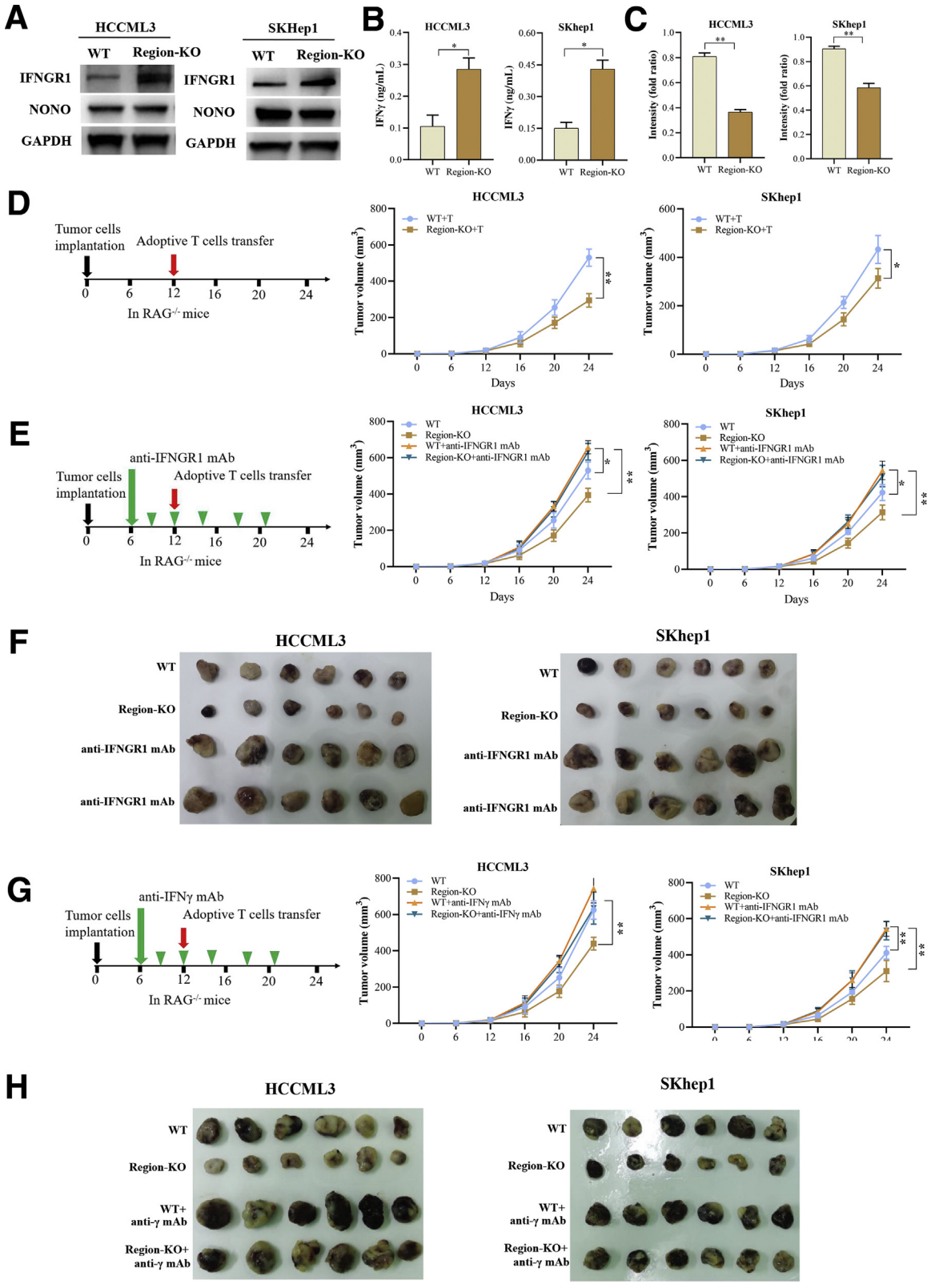

phosphorylated Ser/Thr modification of NONO in HCC cells. We speculate that NEAT1_2, NONO, and other proteins especially phosphokinase may form the complex to regulate phosphorylated modification of NONO, thereby affecting the RNA binding ability of NONO. The detailed phosphokinase involved in regulating phosphorylated modification of NONO needs to be investigated in future studies by mass spectrometry. In addition, SFPQ, which is another core protein of paraspeckle and interacts with NEAT1_2 and NONO, has been reported to induce ISG expression.[41] Whether paraspeckle sequesters protein that affects IFN-γ downstream gene transcription still needs to be explored.

Currently, immunotherapy with immune checkpoint blockade, including nivolumab, pembrolizumab, durvalumab, and tremelimumab, has been applied for advanced HCC therapy in clinical use and has yielded promising results.[7] However, the objective response rate of immunotherapy still needs to be improved. Our results report that paraspeckle expression negatively relates to IFNGR1 in HCC tissues, but paraspeckle does not affect T-cell infiltration in the tumor microenviroment of HCC, hinting that NEAT1_2 highly expressed HCC patient may be more resistant to T-cell therapy in clinic. Thus, NEAT1_2 and NONO may be important factors for guidance to select treatment methods for HCC patients and also as potential targets for HCC therapy.

In conclusion, our results indicate that paraspeckle in HCC cells helps tumor cells escape from immunosurveillance through sequestering IFNGR1 mRNA to inhibiting IFN-γ-IFNGR1 signaling, thereby avoiding T-cell killing effects.

Methods

Cells and Cell Culture

Human HCC cell lines HepG2, Hep3b, BEL7404, Huh7, SKhep1, and PLCPRF5 were all purchased from American Type Culture Collection (ATCC, Manassas, VA). Human normal liver cell line HL7702 and human HCC cell lines BEL7402, BEL7405, HCCLM3, MHCC97h, QGY-7701, QGY-7703, and SMMC-7721 were purchased from Cell Bank of Shanghai Institute of Biochemistry and Cell Biology, Chinese Academy of Sciences (Shanghai, China). All cells were cultured in Dulbecco modified Eagle medium (Thermo Fisher Scientific Inc, Waltham, MA) containing 10% fetal bovine serum (Thermo Fisher Scientific, Inc), 1% penicillin and streptomycin solution at 37°C in an incubator with a humidified atmosphere and 5% CO_2.

Quantitative Real-Time Polymerase Chain Reaction

Total RNA of HCC cells was extracted by using Trizol Reagent (Invitrogen, Carlsbad, CA). RNA from each sample was reverse transcribed into cDNA using the PrimeScript RT reagent kit (TOYOBO, Osaka, Japan). Quantitative real-time polymerase chain reaction (qRT-PCR) was performed by using the Q7 real-time PCR system (Applied Biosystems, Foster City, CA) with SYBR Green Master Mix (TOYOBO). The obtained data were normalized to GAPDH expression levels in each sample. The primers for qRT-PCR are listed in Table 1.

Western Blotting and Co-immunoprecipitation

Western blotting was performed as previously described.[21] Briefly, cells were harvested and lysed using cell lysis buffer (Cell Signaling Technology, Danvers, MA). After measuring the protein concentration using BCA kit (Thermo Fisher), protein was loaded into 10% polyacrylamide sodium dodecyl sulfate gel after transfer onto polyvinylidene difluoride membranes (Millipore, Burlington, MA) and incubated with primary antibodies at 4°C overnight. Polyvinylidene difluoride membranes were washed 3 times with phosphate-buffered saline (PBS) for a total of 15 minutes and incubated with specific secondary antibodies (1:10000; Cell Signaling Technology) for 1 hour at room temperature. Later the signals were detected by using electrochemiluminescence kit (Pierce). Primary antibodies against IFNGR1 (1:1000, ab134070; Abcam, Cambridge, UK), glyceraldehyde-3-phosphate dehydrogenase (1:2000, GAPDH) (ab8245; Abcam), STAT1 (1:1000, 14994; Cell Signal Technology), phosphorylated STAT1 (pSTAT1) (1:1000, 9167; Cell Signal Technology), NONO (1:1000, ab70335; Abcam), flag (1:2000, ab18230; Abcam), Phospho-(Ser/Thr) (1:500, ab117253; Abcam), and Phospho-Tyrosine (P-Tyr) (1:500, 8954; Cell Signal Technology) were used. Co-immunoprecipitation was performed as previously described.[5]

Activated T-Cell–Mediated Tumor Cell Killing Assay

To acquire activated T cells, isolated human peripheral blood lymphocytes were cultured in RPMI 1640 medium (Gibco, Waltham, MA) containing 5% fetal bovine serum, recombinant human interleukin 2 (500 U/mL; PeproTech, Rocky Hill, NJ), anti-CD3-activating antibody (Clone HIT3α; BD Biosciences, Franklin Lakes, NJ), and 10 μg/mL

Figure 10. (***See previous page***). **NEAT1_2 region 13-15 is essential for paraspeckle-mediated T-cell killing tolerance.** (*A*) Western blotting analysis of protein expressions of IFNGR1 and NONO in WT or region 13-15 of NEAT1_2-KO HCCML3 or SKhep1 cells. (*B*) IFN-γ production in cultural supernatants of indicated HCC cells was detected by enzyme-linked immunosorbent assay. (*C*) Response of indicated HCC cells to T-cell–mediated cytolysis was detected by T-cell–mediated tumor cell killing assay. (*D*) Schematic diagram of animal experimental protocols to assess effects of region 13-15 of NEAT1_2-KO on adoptive T-cell anti-tumor immunity in immunodeficient $RAG^{-/-}$ mouse (n = 6). (*E*) Schematic diagram of animal experimental protocols to assess effects of blocking IFNGR1 with anti-IFNGR1 mAb on adoptive T-cell anti-tumor immunity in immunodeficient $RAG^{-/-}$ mouse (n = 6). (*F*) Image showing comparison of excised tumor size of HCC xenografts in RAG1-/- mice. (*G*) Schematic diagram of animal experimental protocols to assess effects of neutralizing IFN-γ with anti-IFN-γ mAb on adoptive T-cell anti-tumor immunity in immunodeficient $RAG^{-/-}$ mouse (n = 6). (*H*) Image showing comparison of excised tumor size of HCCML3 xenografts in RAG1-/- mice. Data are represented as means ± SD (n = 6; $^{*}P < .05$, $^{**}P < .01$).

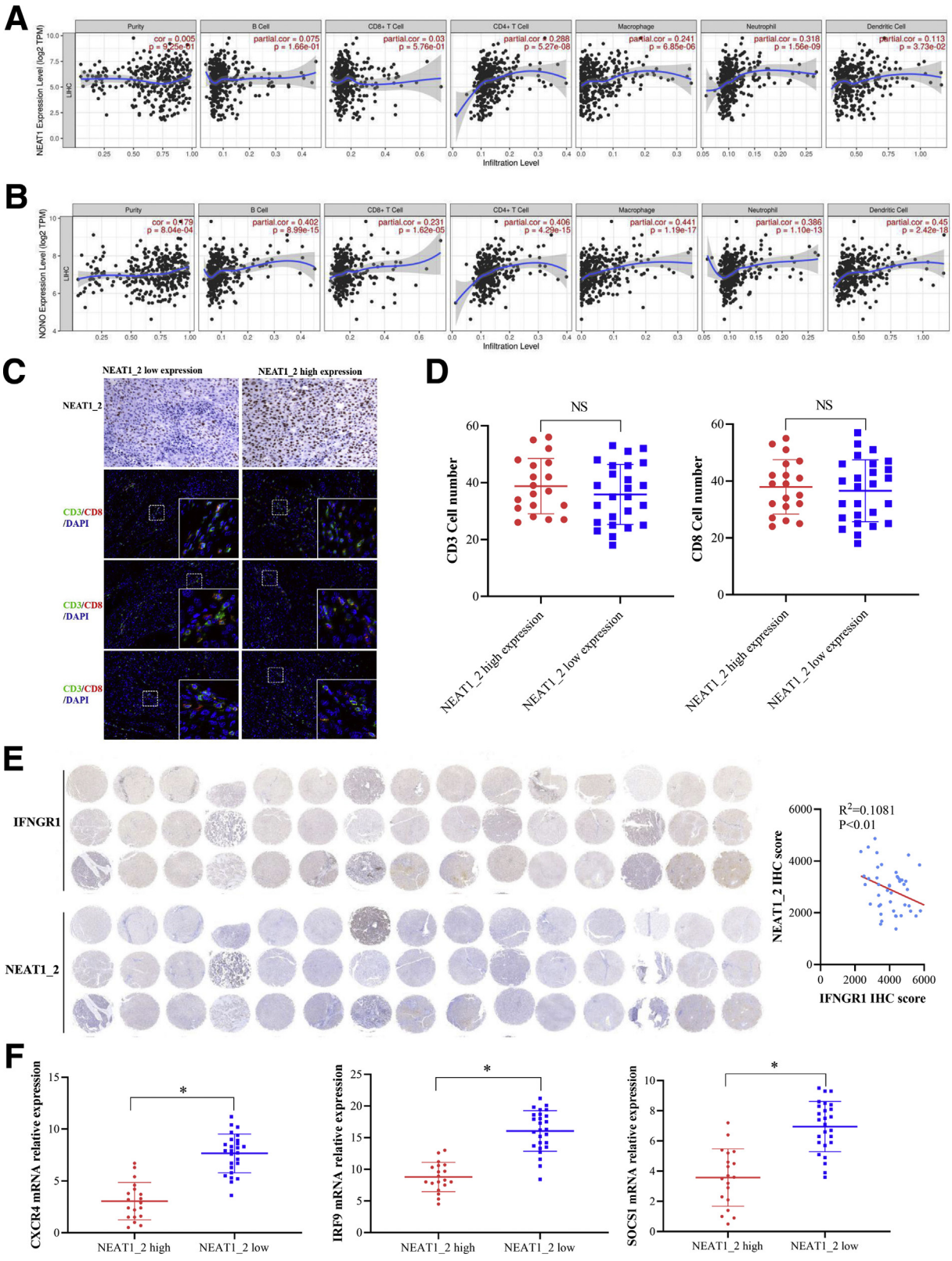

Figure 11. NEAT1_2 expression negatively correlates with IFNGR1 expression in clinical tumor tissues. (*A* and *B*) TIMER analysis of co-relationship between NEAT1, NONO, and immune cell infiltration. (*C*) Immunohistochemistry analysis of NEAT1_2 and immunofluorescence analysis of CD3 (*green*) and CD8 (*red*) expressions in HCC tissues. (*D*) Numbers of $CD3^+$ or $CD8^+$ T cells were calculated. (*E*) Immunohistochemistry analysis of NEAT1_2 and IFNGR1 expressions in HCC tissues (*left*). Correlation analysis of NEAT1_2 expression and IFNGR1 expression in HCC tissues (*right*). (*F*) qRT-PCR analysis of CXCR4, IRF9, and SOCS1 mRNA relative expressions in NEAT1_2 highly/lowly expressed HCC tissues. Data are represented as means ± SD (n = 3; **P* < .05, ***P* < .01).

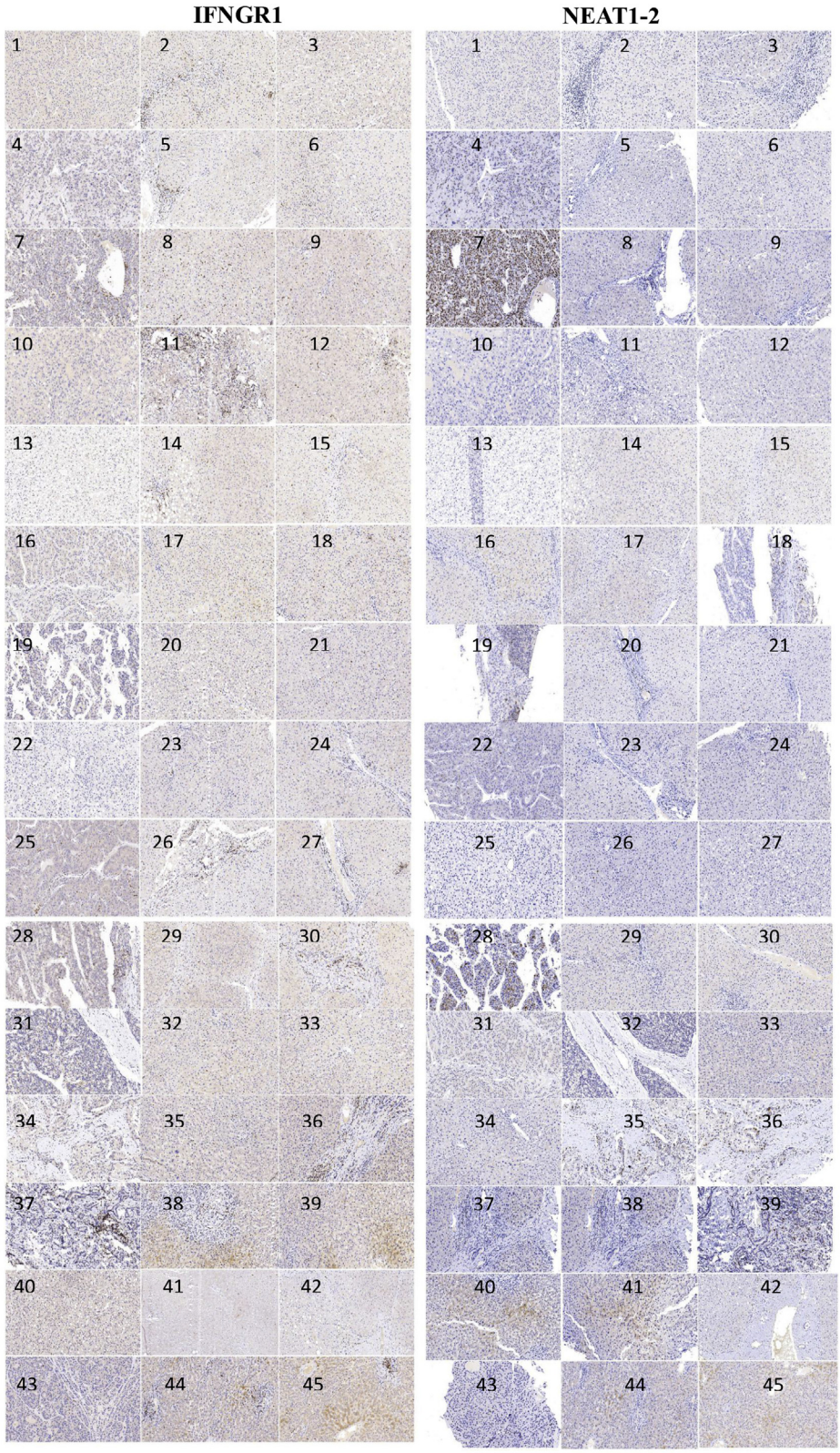

Figure 12. Immunohistochemistry analysis of IFNGR1 and NEAT1_2 expressions in HCC clinicaltissues.

nivolumab (HY-P9903; MCE) for 1 week according to the manufacturer's protocol.[42] HCC cells were allowed to adhere to the plates overnight and then co-cultured with activated T cells in the proportion of 1:5 for 4 days. Then, T cells and cell debris were removed by PBS twice, and the surviving tumor cells were fixed, stained with a crystal

Table 1. Primers Used in This Study

	Sequence	
Primers for NONO constructs		
NONO F	5′-GCCATGGAGGCCCGAATTCGGATGCAGAGTAATAAAACTTTTAACT-3′	pCMV-Flag-NONO
NONO R	5′-GGCCGCGGTACCTCGAGTTAGTATCGGCGACGTTTGTTTG-3′	
N terminal deletion of NONO (ΔN) F	5′-GCCATGGAGGCCCGAATTCGGCGTCTTTTTGTGGGAAATCT-3′	pCMV-Flag-NONO ΔN
N terminal deletion of NONO (ΔN) R	5′-GGCCGCGGTACCTCGAGTTAGTATCGGCGACGTTTGTTTG-3′	
C terminal deletion of NONO (ΔC) F	5′-GCCATGGAGGCCCGAATTCGGATGCAGAGTAATAAAACTTTTAACT-3′	pCMV-Flag-NONO ΔC
C terminal deletion of NONO (ΔC) R	5′-GGCCGCGGTACCTCGAGTTAGTATTCCCTTGAATCCTTCC-3′	
DHBS domain of NONO (DHBS) F	5′-GCCATGGAGGCCCGAATTCGGCGTCTTTTTGTGGGAAATC-3′	pCMV-Flag-NONO DHBS
DHBS domain of NONO (DHBS) R	5′-GGCCGCGGTACCTCGAGTTAGTATTCCCTTGAATCCTTCC-3′	
RRM1 deletion of NONO DHBS domain (DHBSΔRRM1) F	5′-GCCATGGAGGCCCGAATTCGGTCCCTTACAGTTCGAAACCT-3′	pCMV-Flag-NONO DHBSΔRRM1
RRM1 deletion of NONO DHBS domain (DHBSΔRRM1) R	5′-GGCCGCGGTACCTCGAGTTAGTATTCCCTTGAATCCTTCC-3′	
Both RRM1 and RRM2 deletion of NONO DHBS domain (DHBSΔRRM1+2) F	5′-GCCATGGAGGCCCGAATTCGGTTAGATGATGAAGAGGGAC-3′	pCMV-Flag-NONO DHBSΔRRM1+2
Both RRM1 and RRM2 deletion of NONO DHBS domain (DHBSΔRRM1+2) R	5′-GGCCGCGGTACCTCGAGTTAGTATTCCCTTGAATCCTTCC-3′	
Primers for qRT-PCR		
NEAT1_2 F	5′-ACATTGTACACAGCGAGGCA-3′	
NEAT1_2 R	5′-CATTTGCCTTTGGGGTCAGC-3-3′	
IFNGR1 F	5′-TCTTTGGGTCAGAGTTAAAGCCA-3′	
IFNGR1 R	5′-TTCCATCTCGGCATACAGCAA-3′	
S1 RNA-aptamer sequence F	5′-CCGCACTCAGGTTTTGCTTT-3′	
S1 RNA-aptamer sequence R	5′-TGGAAGGAAGCAGCAACACT-3′	
CXCR4 F	5′-ACTACACCGAGGAAATGGGCT-3′	
CXCR4 R	5′-CCCACAATGCCAGTTAAGAAGA-3′	
IRF9 F	5′-GCCCTACAAGGTGTATCAGTTG-3′	
IRF9 R	5′-TGCTGTCGCTTTGATGGTACT-3′	
SOCS1 F	5′-CACGCACTTCCGCACATTC-3′	
SOCS1 R	5′-TAAGGGCGAAAAAGCAGTTCC-3′	
GAPDH F	5′-GGAGCGAGATCCCTCCAAAAT-3′	
GAPDH R	5′-GGCTGTTGTCATACTTCTCATGG-3′	
Sequences of siRNAs		
si-NEAT1_2-1	5′-GAACUCACCUCCUGAUUAUTT-3′	
si-NEAT1_2-2	5′-GGAGGAGUCAGGAGG AAUAUU-3′	
si-NONO	5′-GGGGUGGUAUUAAACAAGUCA-3′	
si-NC	5′-UUCUCCGAACGUGUCACGUTT-3′	
Primers used for RIP		
NEAT1_2 region 1 (R1, 225 bp to 710 bp) F	5′-CTGGTGGAGGGGGAACTTGACC-3′	
NEAT1_2 region 1 (R1, 225 bp to 710 bp) R	5′-CCACATCACTCCTCAGACCA-3′	
NEAT1_2 region 2 (R2, 1135 bp to 187 bp) F	5′-ATGCTTCATGGACCGTGGTT-3′	
NEAT1_2 region 2 (R2, 1135 bp to 1870 bp) R	5′-CTTGTACCCTCCCAGCGTTT-3′	
NEAT1_2 region 3 (R3, 1902 bp to 2179 bp) F	5′-GGCAGGTCTAGTTTGGGCAT-3′	
NEAT1_2 region 3 (R3, 1902 bp to 2179 bp) R	5′-CCTCATCCCTCCCAGTACCA-3′	
NEAT1_2 region 4 (R4, 2833 bp to 3278 bp) F	5′-GATGGGCTCTTCTGGATTTG-3′	
NEAT1_2 region 4 (R4, 2833 bp to 3278 bp) R	5′- ATGTAGTAAAGGCACCTCGCCC-3′	
NEAT1_2 region 5 (R5, 3857 bp to 4460 bp) F	5′-GTAGGAGAGCATGGTAACCAC-3′	
NEAT1_2 region 5 (R5, 3857 bp to 4460 bp) R	5′-GGCAGTGGCTTCCATTCTAC-3′	
NEAT1_2 region 6 (R6, 5286 bp to 5888 bp) F	5′-GTGTTGATGGCAGTGCCAGC-3′	
NEAT1_2 region 6 (R6, 5286 bp to 5888 bp) R	5′-TCAGAGGAAGTTCACAGCCACC-3′	

Table 1. Continued

	Sequence
NEAT1_2 region 7 (R7, 6481 bp to 6960 bp) F	5′-TGCCCAGCAGGGAGGGATTT-3′
NEAT1_2 region 7 (R7, 6481 bp to 6960 bp) R	5′-TTTATGTACTCTTGGGGTGG-3′
NEAT1_2 region 8 (R8, 7145 bp to 7464 bp) F	5′-CAGAAGACCTTGAGGGCAGG-3′
NEAT1_2 region 8 (R8, 7145 bp to 7464 bp) R	5′-AGTGGCTAGACCTGACGCTA-3′
NEAT1_2 region 9 (R9, 8244 bp to 8773 bp) F	5′-CATTCCATTCCCTCCAGCCTCAG-3′
NEAT1_2 region 9 (R9, 8244 bp to 8773 bp) R	5′-CAAGTGTTGGGGAGGATGTG-3′
NEAT1_2 region 10 (R10, 9280 bp to 9549 bp) F	5′-GTTGATGGGCATGTAGGTTGG-3′
NEAT1_2 region 10 (R10, 9280 bp to 9549 bp) R	5′-CATAAGTGGCAAATGTGGCCTTC-3′
NEAT1_2 region 11 (R11, 10269 bp to 1065 1bp) F	5′-CCATGGTGTAGAGATACCAC-3′
NEAT1_2 region 11 (R11, 10269 bp to 10651 bp) R	5′-GAGAGCCATGTTGTGTCCTG-3′
NEAT1_2 region 12 (R12, 11043 bp to 11497 bp) F	5′-TTATGTGGTCCCACACCACCCGCCT-3′
NEAT1_2 region 12 (R12, 11043 bp to 11497 bp) R	5′-AGGGTGGGGGATTGGTAGTG-3′
NEAT1_2 region 13 (R13, 12132 bp to 12749 bp) F	5′-GCATTCATGGGCTTAATGCTG-3′
NEAT1_2 region 13 (R13, 12132 bp to 12749 bp) R	5′-CACCCAGAGGGATGCAAAAGAG-3′
NEAT1_2 region 14 (R14, 13253 bp to 13597 bp) F	5′-CTTCAGGGGCTAAGCACACA-3′
NEAT1_2 region 14 (R14, 13253 bp to 13597 bp) R	5′-GCATTTGCCTTTGGGGTCAG-3′
NEAT1_2 region 15 (R15, 13796 bp to 13934 bp) F	5′-TAAAGCTGTACAGGCGTGGG-3′
NEAT1_2 region 15 (R15, 13796 bp to 13934 bp) R	5′-ACACGGCTACCACACAGATG-3′
NEAT1_2 region 16 (R16, 14495 bp to 14832 bp) F	5′-GAAAAGGCTAATCCAGCTGAAG-3′
NEAT1_2 region 16 (R16, 14495 bp to 14832 bp) R	5′-TGAAGACATCACAGGGAAGG-3′
NEAT1_2 region 17 (R17, 15302 bp to 15689 bp) F	5′-GCCCAACCCCTCAACAGCCTA-3′
NEAT1_2 region 17 (R17, 15302 bp to 15689 bp) R	5′-AGCGTCTGTTTGGGATGACG-3′
NEAT1_2 region 18 (R18, 16347 bp to 16760 bp) F	5′-GCACCTTTGCTGGTGCTGTT-3′
NEAT1_2 region 18 (R18, 16347 bp to 16760 bp) R	5′-TGCACCACCATGCCTGACTA-3′
NEAT1_2 region 19 (R19, 17221 bp to 17602 bp) F	5′-AGGCTGAGGCAGGAGGATCA-3′
NEAT1_2 region 19 (R19, 17221 bp to 17602 bp) R	5′-AGCCTTGAACTCCTGGGCTCA-3′
NEAT1_2 region 20 (R20, 18484 bp to 19130 bp) F	5′-TGGGGCTGGCCTTCTTTTAG-3′
NEAT1_2 region 20 (R20, 18484 bp to 19130 bp) R	5′-AGAGCAAGACTGCCTCACAC-3′
NEAT1_2 region 21 (R21, 20366 bp to 21262 bp) F	5′-TGCATTCTCACCGTCACTCC-3′
NEAT1_2 region 21 (R21, 20366 bp to 21262 bp) R	5′-GGTGCGGGCACTTACTTACT-3′
NEAT1_2 region 22 (R22, 21841 bp to 22409 bp) F	5′-TGGTGCTGTGGACCGTGGAT-3′
NEAT1_2 region 22 (R22, 21841 bp to 22409 bp) R	5′-CTTCAGCTCTCCCTCCCTCT-3′

bp, base pair; F, forward; R, reverse.

Table 2. Clinicopathologic Characteristics of 45 HCC Patients

Variable	No. of patients
Total	45
Age, *y*	
≤60	20
>60	25
Gender	
Male	32
Female	13
Clinical stage	
I-II	19
III-IV	26
Degree of differentiation	
Well/moderate	31
Poor	14
HBV	
Positive	28
Negative	17
Portal hypertension	
Yes	9
No	36
Child-Pugh cirrhosis score	
A	11
B	26
C	8
Indocyanine green retention rate at 15 min (ICGR15)	
≤10%	28
10%–20%	16
>20%	1
Alpha fetoprotein	
≤50 ng/mL	20
50–200 ng/mL	21
200 ng/mL	4

violet solution, and then quantified by a spectrometer at optical density (570 nm).

RNA FISH and Immunofluorescence Microscopy

NONO and the NEAT1_2 RNA FISH assays were performed by using the ViewRNA ISH Cell Assay kit (Affymetrix, Santa Clara, CA) following the protocol of the manufacturer. Detailed procedures were as previously described.[21]

SiRNAs and Transfection

The siRNA and negative control were purchased from IGE Biotechnology (Guangzhou, China). The sequences of si-NEAT1_2-1, si-NEAT1_2-2, si-NONO, and si-NC are listed in Table 1. Transfections were performed with jetPRIME reagent (Polyplus-transfection, Illkirch, France) according to the manufacturer's instructions.

Plasmids

Human NONO gene and truncated NONO domains were amplified and then cloned into pCMV-flag-N-vector as previously described.[43] The pCMV-flag-N-NONO mutant (Ser147 to Ala) was synthesized by IGE Biotechnology. The primers for PCR are listed in Table 1.

Generation of CRISPR-Edited Tumor Cell Lines

For generation of S1-aptamer-tagged 3′ end lncRNA-NEAT1_2 of HCCML3 or SKhep1 cells, we targeted 3′ end of the lncRNA-NEAT1_2 gene to generate a 3′ end fusion of lncRNA-NEAT1_2 with S1-aptamer, using CRISPR/Cas9 genome editing. The S1 RNA aptamer targeting vector was constructed by IGE Biotechnology. The targeting vector contained 80 base pair 3′ end homology region (lncRNA-NEAT1_2 gene), S1 RNA aptamer sequences, and 80 base pair homology region (downstream of 3′ end lncRNA-NEAT1_2 gene). For CRISPR/Cas9 mediated targeting we designed a single guide RNA binding upstream of 3′ end sequence of the lncRNA-NEAT1_2 gene using CRISPOR website (http://crispor.tefor.net). The specific single guide RNA was cloned into the BbsI site of the pU6-(BbsI)-sgRNA-CAG-Cas9-Venus-bpA plasmid (Addgene, plasmid 86986). Approximately 2×10^5 HCCML3 or SKhep1 cells were transfected with jetPRIME reagent to deliver 1.25 μg single guide RNA/Cas9-Venus expressing plasmid and 1.25 μg targeting vector. Cells expressing single guide RNA/Cas9-Venus were selected by sorting highly green fluorescent protein expressing cells using flow cytometry. Cells were seeded at low density to obtain colonies derived from single cells. Single colonies were picked and expanded. Correct insertion of the targeting construct was validated by PCR and Sanger sequencing.

For generation of IFNGR1-KO) HCCML3 or SKhep1 cells, or region-13 to region-15 of lncRNA-NEAT1_2 KO HCCML3 or SKhep1 cells, guide RNA sequences for CRISPR/Cas9 were designed at the CRISPR design web site (http://crispor.tefor.net). Insert oligonucleotides for IFNGR1-KO or NEAT1_2 region-KO gRNAs are AUUGUACACCCUAAUGUAACGUUUUAGAGCUAUGCU or AGGAAUUAGACUCUGGGGCC, respectively. The complementary oligonucleotides for guide RNAs were annealed and cloned into pX459 CRISPR/Cas9-Puro vector (Addgene, Cambridge, MA). HCCML3 or SKhep1 cells were transfected with pX459/gRNA with jetPRIME reagent. Two days after transfection, cells were treated with 1 μg/mL puromycin for 3 days. After 2 weeks, colonies were isolated with the cloning cylinders, and KO clones were validated by DNA sequencing.

RIP

RIP was performed as previously described.[21] Briefly, after treatments, WT HCCML3 or SKhep1 cells or S1-aptamer-tagged (S1 tag) 3′ lncRNA-NEAT1_2 of HCCML3 or SKhep1 cells were harvested and lysed in Polysome lysis buffer (100 mmol/L KCl, 5 mmol/L $MgCl_2$, 10 mmol/L HEPES pH 7.0, 0.5% NP40, 1 mmol/L DTT, 80 U/mL RNase inhibitors, 400 μmol/L VRC, and protease inhibitors cocktail) for 30 minutes on ice. Lysates were sonicated to fragment chromatins and RNAs and centrifuged, and protein concentration in the supernatant was measured with BCA assay (Thermo Fisher). Proteins were incubated with

Protein G-coupled Magnetic Dynabeads (Life Technologies, Carlsbad, CA) pre-coated with rabbit anti-NONO antibody (ab70335; Abcam) or immunoglobulin G control or incubated with Dynabeads MyOne Streptavidin C1 magnetic beads (Invitrogen) for 4 hours at 4°C. Before the incubation, one tenth of the supernatant was put aside to be used as input. After incubation, samples were washed 5 times with NT buffer (50 mmol/L Tris-HCl pH 7.4, 150 mmol/L NaCl, 1 mmol/L $MgCl_2$, 1% Triton X-100). Immunoprecipitated RNAs and input RNAs were isolated by TRIzol (Invitrogen), incubated with DNase I (Sigma-Aldrich, St. Louis, MO), reverse-transcribed into cDNA, and subjected to qRT-PCR detection. The RIP primers are listed in Table1. For the RIP-seq analysis, RNA-seq was performed at Novogene (Beijing, China), and reads uniquely mapped to the genome were subjected to calling the peaks in the enriched regions with a fold enrichment of at least 2 over input reads.

Flow Cytometry

After treatment, HCCML3 or SKhep1 cells were suspended, washed, then stained with fluorescein isothiocyanate–conjugated anti-IFNGR1 antibodies (ab11286; Abcam) or mouse immunoglobulin G (ab99763; Abcam) for 30 minutes at 4°C, and then washed again. Flow cytometry was carried out with LSRII flow cytometer (BD Biosciences, San Jose, CA), and data were analyzed with FlowJo software (v.10.4; Tree Star, San Carlos, CA).

Nuclear/Cytosol RNA Fractionation

Nuclear/cytosol RNA fractionation was isolated by nuclear/cytosol fractionation kit (Biovision Inc, Milpitas, CA) as previously described.[21] Briefly, cells were homogenized in cell fractionation buffer thoroughly before centrifuged for 5 minutes at 1500 rpm. Supernatant was collected as cytosolic fraction, whereas nuclear pellet was washed and lysed by cell disruption buffer. Such samples were mixed with 2× lysis/binding solution before extracting RNA according to the manufacturer's protocol.

In Situ Hybridization

Paraffin-embedded sections of human HCC tissues were deparaffinized with xylene and rehydrated with 100%, 90%, 70%, and 50% ethanol (5 minutes each) at room temperature. The samples were digested with proteinase K and fixed in 4% paraformaldehyde for 10 minutes at room temperature, followed by hybridization with the NEAT1_2 probe (GenePharma, Shanghai, China) at 55°C overnight and subsequent incubation with horseradish peroxidase–conjugated secondary antibody for 30 minutes at 4°C. Diaminobenzidine was used to develop the stain with a colorimetric reaction for 30 minutes at room temperature, and then the sections were observed under light microscope.

Immunohistochemistry

Paraffin-embedded sections of human HCC tissues were dewaxed with 100%, 90%, 70%, and 50% alcohol solutions (5 minutes each at 37°C), followed by heat-induced repair in 0.01 mol/L citrate buffer (pH 6.0), 20 minutes of endogenous peroxidase inhibition with 0.3% hydrogen peroxide, 30 minutes of incubation at room temperature in 20% normal goat serum, and overnight incubation at 4°C with anti-IFNGR1 (1:100, ab134070; Abcam), anti-CD3 (1:100, 17617-1-AP; Proteintech, Rosemont, IL), or anti-CD8 (1:100, 1G2B10; Proteintech) antibody. The sections were then incubated for an additional 1 hour at 37°C, washed with 0.01 mol/L PBS, and incubated for 20 minutes at 37°C with horseradish peroxidase–conjugated secondary antibody. After development with 3,3′-diaminobenzidine reagent for 5 minutes at room temperature, sections were observed for staining under a light microscope. Finally, hematoxylin was used for 30 seconds of counterstaining; sections were then rinsed with running water for 5 minutes, hyalinized, and mounted with neutral resin before observation under light microscope.

IFN-γ Treatment

HCCML3 or SKhep1 cells were stimulated with 100 ng/mL recombinant human IFN-γ (300-02; PeproTech) dissolved in 0.1% bovine serum albumin for 0, 15, or 30 minutes or 0, 6, or 12 hours at 37°C. Cells were then processed for further analysis.

Immune Association Analysis

Association between immune infiltrates and NEAT1/NONO expressions in HCC was analyzed by TIMER (http://timer.cistrome.org/).

Enzyme-Linked Immunosorbent Assay

IFN-γ protein expression levels in culture supernatants of HCC cells were collected and measured using an interferon gamma human ELISA kit (ab100537; Abcam) according to the manufacturer's instructions.

Study Approval

All animal experiments were approved by Westlake University. HCC samples were acquired from Shengjing Hospital of China Medical University. This study was approved by the ethics committee of Westlake University and Shengjing Hospital of China Medical University, and all participants signed informed consent forms in this study. No patients had received chemotherapy or radiotherapy before surgery.

In Vivo Tumor Progression and Immunotherapy Models

Immunodeficient RAG1-/- mice (B6;129-*Rag1tm1Smoc*) were obtained from Shanghai Model Organisms (China). All animals were maintained under standardized conditions at 21°C and a 12-hour light cycle, with free access to food and water. 2×10^6 HCC cells (in 100 μL PBS) were subcutaneously transplanted into the back flanks of 5- to 6-week-old RAG1-/- mice. Mice were randomly separated into different groups ($n = 6$). For the adoptive T-cell immunotherapy model, activated T cells (1×10^7 T cells/mouse)

were intravenously transfused into tumor-bearing mice at day 12. Anti-IFNGR1 antibodies (200 μg/mouse) or neutralizing mAb against IFN-γ (Bio X Cell, Lebanon, NH) (200 μg/mouse) were intraperitoneally injected into tumor-bearing mice 3 times per week for 2 weeks after tumor implantation. AAV-expressing shRNA-against NEAT1_2 (AAV-shR-NEAT1_2, 2×10^8 TU/10 μL), constructed by GenePharma (Shanghai, China), were injected intravenously (injection 5 times every 4 days). After 24 days, mice were killed, and tumor dimensions were measured with vernier calipers, and volumes were calculated as follows: tumor volume (mm^3) = [width^2 (mm^2) $\times$ length (mm)]/2. Tumor dimension was measured on day 0 before treatment and days 2, 4, and 6 after initiation of treatment. All measurements were conducted in a blinded fashion.

Statistical Analysis

To identify the significant differences between 2 groups, a Student t test was used. For correlation analysis between 2 continuous variables, r values represent Pearson's correlation coefficients, and P values were calculated by Pearson's correlation test. Statistical analyses were performed with GraphPad (San Diego, CA) version 5.0. Statistical significance was shown as $^{**}P < .01$ or $^{*}P < .05$.

References

1. Yi PS, Wang H, Li JS. Evolution and current status of the subclassification of intermediate hepatocellular carcinoma. World J Gastrointest Surg 2020;12:85–92.
2. Refolo MG, Messa C, Guerra V, Carr BI, D'Alessandro R. Inflammatory mechanisms of HCC development. Cancers (Basel) 2020;12.
3. Kishore SA, Bajwa R, Madoff DC. Embolotherapeutic strategies for hepatocellular carcinoma: 2020 update. Cancers (Basel) 2020;12.
4. Gbolahan OB, Schacht MA, Beckley EW, LaRoche TP, O'Neil BH, Pyko M. Locoregional and systemic therapy for hepatocellular carcinoma. J Gastrointest Oncol 2017;8:215–228.
5. Sindhi R, Rohan, Bukowinski A, Tadros S, de Ville de Goyet J, Rapkin L, Ranganathan S. Liver transplantation for pediatric liver cancer. Cancers (Basel) 2020;12.
6. Belizario J, Destro Rodrigues MF. Checkpoint inhibitor blockade and epigenetic reprogrammability in CD8(+) T-cell activation and exhaustion. Ther Adv Vaccines Immunother 2020;8:2515135520904238.
7. Nakano S, Eso Y, Okada H, Takai A, Takahashi K, Seno H. Recent advances in immunotherapy for hepatocellular carcinoma. Cancers (Basel) 2020;12.
8. Green AK, Feinberg J, Makker V. A review of immune checkpoint blockade therapy in endometrial cancer. Am Soc Clin Oncol Educ Book 2020;40:187.
9. Bu X, Yao Y, Li X. Immune checkpoint blockade in breast cancer therapy. Adv Exp Med Biol 2017;1026:383–402.
10. Zhang JC, Chen WD, Alvarez JB, Jia K, ShiL, Wang Q, Zou N, He K, Zhu H. Cancer immune checkpoint blockade therapy and its associated autoimmune cardiotoxicity. Acta Pharmacol Sin 2018;39:1693–1698.
11. Salerno F, Turner M, Wolkers MC. Dynamic post-transcriptional events governing CD8(+) T cell homeostasis and effector function. Trends Immunol 2020;41:240–254.
12. Liu J, Jaijyan DK, Tang Q, Zhu H. Promising cytomegalovirus-based vaccine vector induces robust CD8(+) T-cell response. Int J Mol Sci 2019;20.
13. El-Khoueiry A, Sangro B, Yau T, Crocenzi TS, Kudo M, Hsu C, Kim TY, Choo SP, Trojan J, Welling THR, Meyer T, Kang YK, Yeo W, Chopra A, Anderson J, Dela Cruz C, Lang L, Neely J, Tang H, Dastani HB, Melero I. Nivolumab in patients with advanced hepatocellular carcinoma (CheckMate 040): an open-label, non-comparative, phase 1/2 dose escalation and expansion trial. Lancet 2017;389:2492–2502.
14. Tella SH, Mahipal A, Kommalapati A, Jin Z. Evaluating the safety and efficacy of nivolumab in patients with advanced hepatocellular carcinoma: evidence to date. Onco Targets Ther 2019;12:10335–10342.
15. Pisani G, Baron B. Nuclear paraspeckles function in mediating gene regulatory and apoptotic pathways. Noncoding RNA Res 2019;4:128–134.
16. Yamazaki T, Souquere S, Chujo T, Kobelke S, Chong YS, Fox AH, Bond CS, Nakagawa S, Pierron G, Hirose T. Functional domains of NEAT1 architectural lncRNA induce paraspeckle assembly through phase separation. Mol Cell 2018;70:1038–1053 e1037.
17. Hennig S, Kong G, Mannen T, Sadowska A, Kobelke S, Blythe A, Knott GJ, Iyer KS, Ho D, Newcombe EA, Hosoki K, Goshima N, Kawaguchi T, Hatters L, Trinkle-Mulcahy L, Hirose T, Bond CS, Fox AH. Prion-like domains in RNA binding proteins are essential for building subnuclear paraspeckles. J Cell Biol 2015;210:529–539.
18. Yang F, Tang Z, Duan A, Yi B, Shen N, Bo Z, Yin L, Zhu B, Qiu Y, Li J. Long noncoding RNA NEAT1 upregulates survivin and facilitates gallbladder cancer progression by sponging microRNA-335. Onco Targets Ther 2020;13:2357–2367.
19. Knutsen E, Lellahi SM, Aure MR, Nord S, Fismen S, Larsen KB, Gabriel MT, Hedberg A, Bjorklund SS, Oslo C, Breast Cancer Research, Bofin AM, Maelandsmo GM, Sorlie T, Mortensen ES, Perander M. The expression of the long NEAT1_2 isoform is associated with human epidermal growth factor receptor 2-positive breast cancers. Sci Rep 2020;10:1277.
20. Liu F, Ai FY, Zhang DC, Tian L, Yang ZY, Liu SJ. LncRNA NEAT1 knockdown attenuates autophagy to elevate 5-FU sensitivity in colorectal cancer via targeting miR-34a. Cancer Med 2020;9:1079–1091.
21. Wang S, Zhang Q, Wang Q, Shen Q, Chen X, Li Z, Zhou Y, Hou J, Xu B, Li N, Cao X. NEAT1 paraspeckle promotes human hepatocellular carcinoma progression by strengthening IL-6/STAT3 signaling. Oncoimmunology 2018;7:e1503913.
22. Kessler SM, Hosseini K, Hussein UK, Kim KM, List M, Schultheiss CS, Schulz MH, Laggai S, Jang KY, Kiemer AK. Hepatocellular carcinoma and nuclear paraspeckles: induction in chemoresistance and prediction for poor survival. Cell Physiol Biochem 2019;52:787–801.

23. Ma F, Lei YY, Ding MG, Luo LH, Xie YC, Liu XL. LncRNA NEAT1 interacted with DNMT1 to regulate malignant phenotype of cancer cell and cytotoxic T cell infiltration via epigenetic inhibition of p53, cGAS, and STING in lung cancer. Front Genet 2020;11:250.
24. Gao J, Shi LZ, Zhao H, Chen J, Xiong L, He Q, Chen T, Roszik J, Bernatchez C, Woodman SE, Chen L, Hwu P, Allison JP, Futreal A, Wargo JA, Sharma P. Loss of IFN-gamma pathway genes in tumor cells as a mechanism of resistance to anti-CTLA-4 therapy. Cell 2016; 167:397–404 e399.
25. Abiko K, Matsumura N, Hamanishi J, Horikawa N, Murakami R, Yamaguchi K, Yoshioka Y, Baba T, Konishi I, Mandai M. IFN-gamma from lymphocytes induces PD-L1 expression and promotes progression of ovarian cancer. Br J Cancer 2015;112:1501–1509.
26. Ahmed CM, Johnson HM. IFN-gamma and its receptor subunit IFNGR1 are recruited to the IFN-gamma-activated sequence element at the promoter site of IFN-gamma-activated genes: evidence of transactivational activity in IFNGR1. J Immunol 2006;177:315–321.
27. West JA, Mito M, Kurosaka S, Takumi T, Tanegashima C, Chujo T, Yanaka K, Kingston RE, Hirose T, Bond C, Fox A, Nakagawa S. Structural, super-resolution microscopy analysis of paraspeckle nuclear body organization. J Cell Biol 2016;214:817–830.
28. Duvignaud JB, Bedard M, Nagata T, Muto Y, Yokoyama S, Gagne SM, Vincent M. Structure, dynamics, and interaction of p54(nrb)/NonO RRM1 with 5′ splice site RNA sequence. Biochemistry 2016;55:2553–2566.
29. Lee HW, Cho KJ, Park JY. Current status and future direction of immunotherapy in hepatocellular carcinoma: what do the data suggest? Immune Netw 2020;20:e11.
30. Wang L, Wang FS. Clinical immunology and immunotherapy for hepatocellular carcinoma: current progress and challenges. Hepatol Int 2019;13:521–533.
31. Busato D, Mossenta M, Baboci L, Di Cintio F, Toffoli G, Dal Bo M. Novel immunotherapeutic approaches for hepatocellular carcinoma treatment. Expert Rev Clin Pharmacol 2019;12:453–470.
32. Dong P, Xiong Y, Yue J, Hanley SJB, Kobayashi N, Todo Y, Watari H. Long non-coding RNA NEAT1: a novel target for diagnosis and therapy in human tumors. Front Genet 2018;9:471.
33. Xia TF, Chen J, Wu K, Zhang J, Yan Q. Long noncoding RNA NEAT1 promotes the growth of gastric cancer cells by regulating miR-497-5p/PIK3R1 axis. Eur Rev Med Pharmacol Sci 2019;23:6914–6926.
34. Xiong Y, Liu Z, Li Z, Wang S, Shen N, Xin Y, Huang T. Long noncoding RNA nuclear paraspeckle assembly transcript 1 interacts with microRNA107 to modulate breast cancer growth and metastasis by targeting carnitine palmitoyltransferase1. Int J Oncol 2019;55:1125–1136.
35. Li Y, Ding X, Xiu S, Du G, Liu Y. LncRNA NEAT1 promotes proliferation, migration and invasion via regulating miR-296-5p/CNN2 axis in hepatocellular carcinoma cells. Onco Targets Ther 2019;12:9887–9897.
36. Wang ZW, Hu X, Ye M, Lin M, Chu M, Shen X. NEDD4 E3 ligase: functions and mechanism in human cancer. Semin Cancer Biol 2020.
37. Fan CD, Lum MA, Xu C, Black JD, Wang X. Ubiquitin-dependent regulation of phospho-AKT dynamics by the ubiquitin E3 ligase, NEDD4-1, in the insulin-like growth factor-1 response. J Biol Chem 2013;288: 1674–1684.
38. Ni JM, Ni AP. Landscape of PD-1/PD-L1 regulation and targeted immunotherapy. Chin Med Sci J 2018; 33:174–182.
39. Chen LL, DeCerbo JN, Carmichael GG. Alu element-mediated gene silencing. EMBO J 2008;27:1694–1705.
40. Bruelle C, Bedard M, Blier S, Gauthier M, Traish AM, Vincent M. The mitotic phosphorylation of p54(nrb) modulates its RNA binding activity. Biochem Cell Biol 2011;89:423–433.
41. Imamura K, Imamachi N, Akizuki G, Kumakura M, Kawaguchi A, Nagata K, Kato A, Kawaguchi Y, Sato H, Yoneda M, Kai C, Yada T, Suzuki Y, Yamada T, Ozawa T, Kaneki K, Inoue T, Kobayashi M, Kodama T, Wada Y, Sekimizu K, Akimitsu N. Long noncoding RNA NEAT1-dependent SFPQ relocation from promoter region to paraspeckle mediates IL8 expression upon immune stimuli. Mol Cell 2014;53:393–406.
42. Ding G, Shen T, Yan C, Zhang M, Wu Z, Cao L. IFN-gamma down-regulates the PD-1 expression and assist nivolumab in PD-1-blockade effect on CD8+ T-lymphocytes in pancreatic cancer. BMC Cancer 2019;19:1053.
43. Zan J, Zhang H, Gu AP, Zhong KL, Lu MY, Bai XX, Zhang JY, Cai J. Yin Yang 1 dynamically regulates antiviral innate immune responses during viral infection. Cell Physiol Biochem 2017;44:607–617.

Received July 16, 2020. Accepted February 19, 2021.

Correspondence
Address correspondence to: Zhi Huang, PhD, Department of Interventional Radiology, Affiliated Hospital of Guizhou Medical University, 16 Beijing Road, Guiyang 550002, China. e-mail: doctor@huangzhicom; or Shuai Wang, PhD, School of Life Sciences, Westlake University, 18 Shilongshan Road, Hangzhou, Zhejiang 310024, China. e-mail: wangshuai@westlake.edu.cn.

CRediT Authorship Contributions

Jie Zan (Conceptualization: Equal; Data curation: Equal; Investigation: Equal; Methodology: Equal; Writing – original draft: Equal)

Xuya Zhao (Investigation: Equal; Methodology: Equal; Resources: Equal)

Xiya Deng (Investigation: Supporting; Methodology: Supporting; Resources: Supporting)

Hongda Ding (Investigation: Supporting; Methodology: Supporting)

Bi Wang (Conceptualization: Equal; Investigation: Equal; Resources: Equal; Writing – original draft: Equal)

Minyi Lu (Conceptualization: Equal; Investigation: Equal; Methodology: Equal; Software: Equal)

Zijing Wei (Conceptualization: Equal; Formal analysis: Equal; Methodology: Equal; Software: Equal)

Zhi Huang (Conceptualization: Equal; Data curation: Equal; Formal analysis: Equal; Investigation: Equal; Methodology: Equal; Project administration: Equal; Supervision: Equal; Writing – original draft: Equal; Writing – review & editing: Equal)

Shuai Wang (Conceptualization: Equal; Data curation: Equal; Formal analysis: Equal; Funding acquisition: Equal; Investigation: Equal; Methodology: Equal; Software: Equal; Writing – original draft: Equal; Writing – review & editing: Equal)

Conflicts of interest
The authors disclose no conflicts.

Funding
Supported by Zhejiang Provincial Natural Science Foundation of China (No. LQ20C070002), National Natural Science Foundation of China (No. 82003045), and Special Funds for the Central Government to Guide Local Science and Technology Development (No. QKZYD[2019]4008).